UNIVERSITÀ
DI SIENA
1240

Department of Medical Biotecnology

PhD in Genetic, Oncology e Clinical Medicine (GenOMeC)

38° Cycle

Coordinator: Professor Ilaria Meloni

MAPK15 modulates NRF2 activity and the expression of its target genes: a novel mechanism for cellular responses to oxidative stress

Scientific Disciplinary Sector: MED/03

Candidate
Giulia Vallini
Place of activity
Azienda Ospedaliero-universitaria Senese
Istituto di Fisiologia Clinica-Consiglio Nazionale delle Ricerche (CNR) of Siena

Firma digitale della candidata

Firmato digitalmente da Giulia Vallini
Data: 04.12.2025 16:04:01 CET

Supervisor
Professor Pietro Rubegni
Università degli Studi di Siena
Co-supervisor
Dr. Mario Chiariello
Istituto di Fisiologia Clinica-Consiglio Nazionale delle Ricerche (CNR)

Academic year of PhD completion
2024/25

Indice

1. Abstract

Reactive Oxygen Species (ROS) are not deleterious for cells when they are maintained at low level, indeed they fulfill important signaling function. However, a substantial increase in ROS can disrupt redox homeostasis and, consequently, lead to oxidative stress that is correlated to numerous human diseases, including tumors. The nuclear factor erythroid 2–related factor 2 (NRF2) is the master regulator of cellular antioxidant responses, activating the transcription of genes that protect the cell from damage caused by free radicals, toxins, and environmental stressors. This protective role is essential for maintaining genome integrity, thereby acting as a tumor suppressor. However, in many advanced cancers, especially non-small cell lung cancer (NSCLC), NRF2 is chronically hyperactivated and this persistent activation has pro-tumorigenic effects, conferring resistance to oxidative stress and chemotherapeutic drugs, promoting cell proliferation, survival, and tumor progression.

Here, we show that endogenous mitogen-activated protein kinase 15 (MAPK15) phosphorylates NRF2, promoting its stabilization at protein level and its nuclear translocation, sustaining, in turn, NRF2 transcriptional activity and the consequent expression of cytoprotective antioxidant genes. On the contrary, when MAPK15 is downregulated, the cell does not properly respond to oxidative insult and ROS and DNA damage increase.

This novel MAPK15-dependent mechanism could be an interesting target for pharmacological or genetic therapies against diseases correlated to oxidative stress. Still, for future applicability, the specific mechanism of modulation must be always evaluated based on the biological context, since the upregulation of MAPK15, and the consequent maintenance of the antioxidant response may both protects against ROS and DNA damage, thereby potentially preventing tumorigenesis, but it may also be deleterious in some pathological contexts where NRF2 upregulation supports cancer development and drug resistance.

2. Abbreviations

The following list contains the abbreviations and acronyms used in this thesis in alphabetical order:

ARE	antioxidant response elements
CSE	condensed smoke extracts
CHX	cycloheximide
DMF	dimethyl fumarate
EPHX1	epoxide hydrolase 1
ERK	extracellular signal-regulated kinase
FACS	fluorescence-activated cell sorting
FBS	fetal bovine serum
FCCP	carbonyl cyanide 4-(trifluoromethoxy) phenylhydrazone
GCLC	glutamate-cysteine ligase catalytic subunit
GCLM	glutamate-cysteine ligase modifier subunit
GeoMFI	geometric mean fluorescent intensity
hAEC	human airway epithelial cells
H2A.X	H2A histone family member X
H_2O_2	hydrogen peroxide
HO-1	heme oxygenase 1
JNK	c-Jun N-terminal kinases
KD	kinase-dead
MAPK15	mitogen activated protein kinase 15
MGST1	microsomal glutathione S-transferase 1
MT2	metallothionein-2
NQO1	NAD(P)H dehydrogenase [quinone] 1
NRF2	NF-E2-Related Factor 2
PCA	principal component analysis
ROS	reactive oxygen species
RT-qPCR	quantitative reverse transcription polymerase chain reaction
SDC	sodium deoxycholate
siMAPK15	MAPK15 specific siRNA
SFN	sulforaphane
siSCR	scrambled siRNA
SOD3	extracellular superoxide dismutase [Cu–Zn]
TPA	12-O-tetradecanoylphorbol-13-acetate
UGT1A6	UDP-glucuronosyltransferase 1-6
ULK1	Unc-51 like autophagy activating kinase 1
WB	wester blot
WT	wild-type

3. Introduction

2.1. MAPK protein family

Mitogen-activated protein kinases (MAPKs) are a family of 14 genes possessing kinase activity directed to serine/threonine residues and activated by extracellular stimuli. The MAPKs family is divided into conventional and atypical groups. The conventional MAPKs family includes four subfamilies of MAPKs, denominated, i) extracellular signal-regulated kinases (ERKs, comprising ERK1 and ERK2 isoforms), ii) ERK5, separated from ERK1/2 for its unique structural features (Nishimoto & Nishida, 2006) iii) c-Jun amino (N)-terminal kinases (JNK, comprising JNK1, JNK2 and JNK3 isoforms) and iv) p38 (comprising p39α, p38β, p38γ and p38δ isoforms). The atypical MAPKs group includes ERK3, ERK4, ERK7/8 and Nemo-like kinase (NLK) (Cargnello and Roux, 2011).
Recently, specific synonyms have been recommended for each member of the family by the HUGO Gene Nomenclature Commitee and Protein Knowledgebase of UniProt (**Table 1**).

Classical nomenclature	Recommended nomenclature
ERK2	MAPK1
ERK1	MAPK3
ERK4	MAPK4
ERK3	MAPK6
ERK5	MAPK7
JNK1	MAPK8
JNK2	MAPK9
JNK3	MAPK10
p38β	MAPK11
p38γ	MAPK12
p38δ	MAPK13
p38α	MAPK14
ERK7/8	MAPK15

Table 1 Recommended nomenclature of MAPKs family members by HUGO Gene Nomenclature Commitee and Protein Knowledgebase of UniProt.

Conventional MAPKs are part of an evolutionary conserved signaling cascade formed by three kinases that act sequentially: a MAPK, a MAPK kinase (MAPKK), and a MAPKK kinase (MAPKKK). MAPKs phosphorylation, leading to their activation, occurs on threonine and tyrosine residues within a conserved Thr-X-Tyr motif located in the kinase domain. On the other hand, there

is still no evidence of the existence of upstream cascades leading to the activation of atypical MAPKs. Moreover, their structures often differ from the conventional ones (**Fig. 1**) (Cargnello & Roux, 2011).

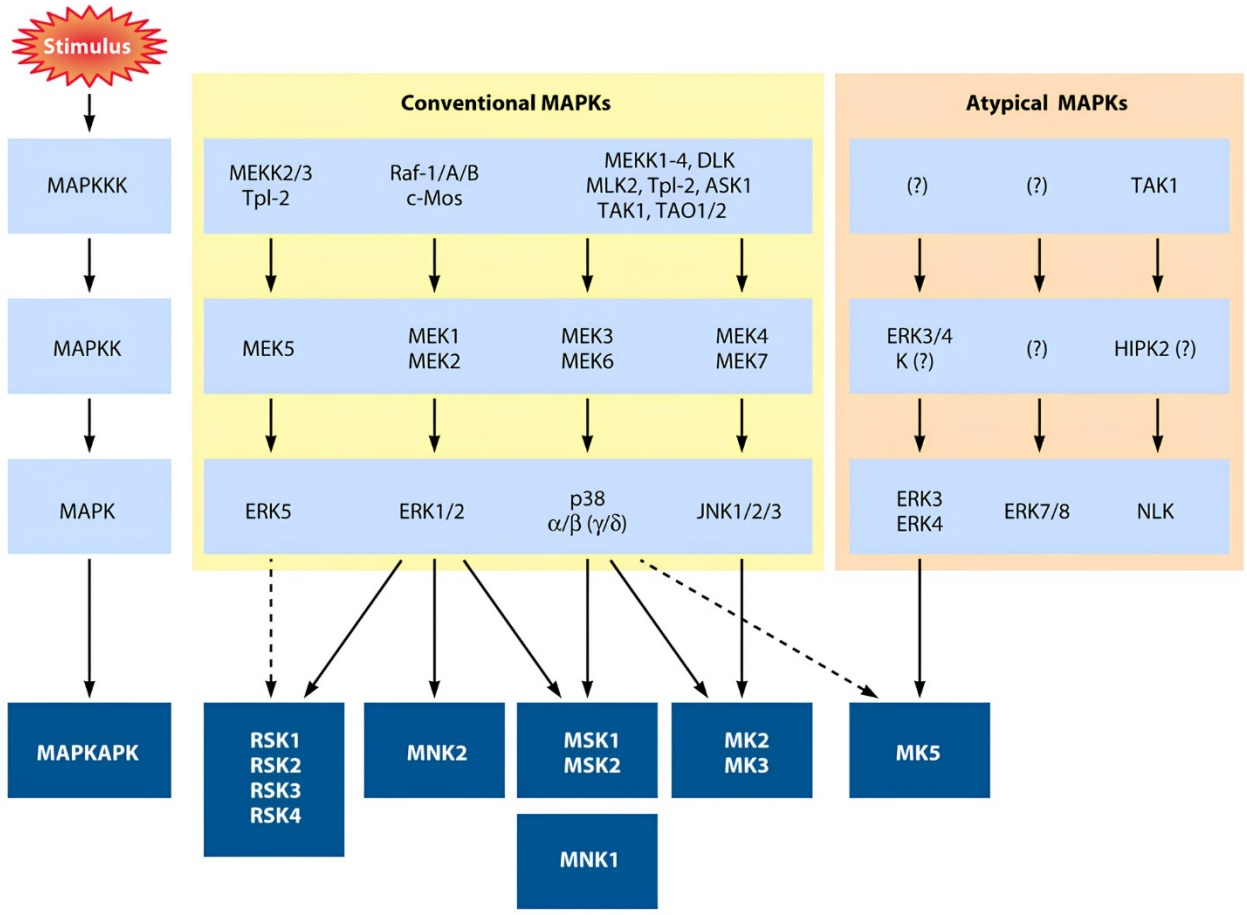

Fig. 1 Schematic representation of MAPKs signaling cascade (Cargnello & Roux, 2011).

Importantly, MAPKs are involved in numerous fundamental signaling pathways, such as proliferation (Parascandolo *et al*., 2024), differentiation (Ozturk *et al*., 2024; W. Wang *et al*., 2024), stress responses (W. Liu *et al*., 2024; Rosette & Karin, 1996), inflammation (Shi *et al*., 2025; Shin *et al*., 2021) and apoptosis (Graves *et al*., 1996; Jeon *et al*., 2023), and for this reason, they are often involved in different pathologies, including cancer (Braicu *et al*., 2019).

2.2. Reactive oxygen species and oxidative stress

Gerschman and coll. initially described the deleterious effects of the exposure to elevated concentration of oxygen *in vivo* causing high free-radical formation (Gerschman *et al*., 1954). Then, in 1995 Davies cleverly described the "Oxygen Paradox": eukaryotic aerobic organism cannot live without oxygen, yet oxygen can be dangerous for their lives (Davies, 1995). Reactive oxygen species (ROS), molecules chemically reactive containing oxygen, include superoxide anion radical, (O_2•−), the hydroxyl radical (•OH), the peroxyl radical (ROO•), and the alkoxyl radical (RO•). Instead, non-radical ROS include hydrogen peroxide (H_2O_2), organic hydroperoxides (ROOH), singlet molecular oxygen ($^1O_2$), electronically excited carbonyl, ozone (O_3), hypochlorous acid (HOCl), and hypobromous acid (HOBr). The principal cellular source of ROS, especially the superoxide anion, is the process of oxidative phosphorylation, occurring in mitochondria. During this process a small

fraction of oxygen molecules may "escape" from respiratory chain enzymes and undergo incompletely reduction (Sarniak *et al*., 2016). There are also exogenous sources of ROS. Among them, there are pollutants, including cigarette smoke (Seo *et al*., 2023) and $PM_{2.5}$ particles (Daiber *et al*., 2020) ultraviolet (UV) radiations (de Jager *et al*., 2017) and drugs (Li *et al*., 2023).

ROS are not deleterious for cells when are maintained at low level, indeed they fulfill important signaling functions. For example, they regulate protein functions by the oxidation of cystine residues (Van Der Reest *et al*., 2018) and are mediators in physiological cell proliferation (Vara & Pula, 2014), differentiation (Nit *et al*., 2021) and migration (Hurd *et al*., 2012) processes. But, when they accumulate in excessive amounts, they can break redox homeostasis.

Redox homeostasis is the maintenance of a balance between oxidizing and reducing reactions within the cell. When reducing reactions cannot contrast with the oxidizing ones, oxidative stress starts and the redox homeostasis gets broken. Cellular damage triggered by oxidative stress can lead numerous human diseases, such as Parkinson's disease (Dias *et al*., 2013), Alzheimer's disease (Luca *et al*., 2015) and cancers (Khan *et al*., 2021). Indeed, excessive ROS lead to genome instability, epigenetic alterations and to the dysregulation of the same signaling pathways mentioned above, otherwise finely regulated in physiological conditions. For example, ROS can activate MAPK and NK-kB signaling pathways, known to promote metastasis by enhancing epithelial-to-mesenchymal transition, cell migration, invasion, cell growth, survival and angiogenesis (Diebold & Chandel, 2016; Khan *et al*., 2021) (**Fig. 2**).

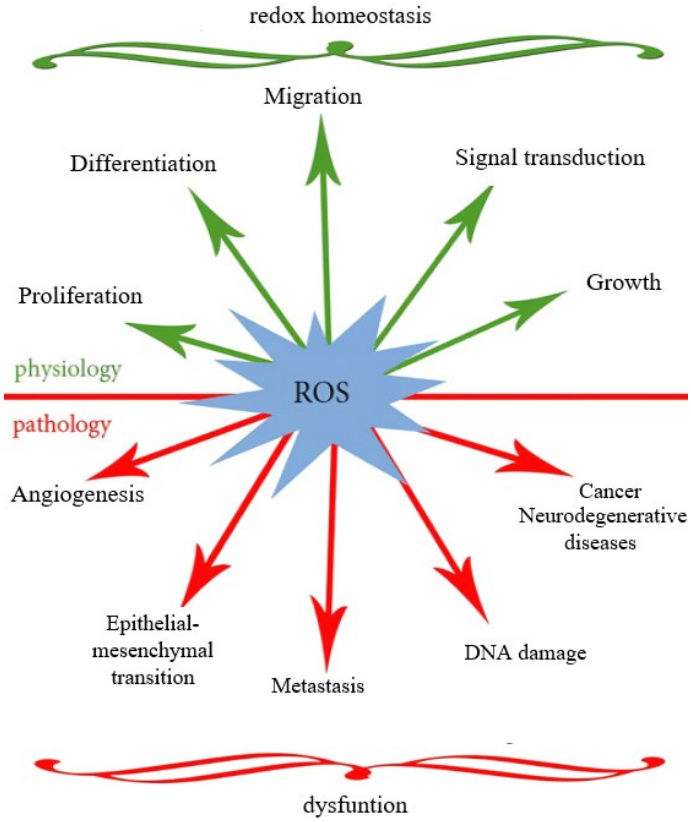

Fig. 2 Role of ROS in physicological and dyregulated conditions (image modified from a picture of Dymkowska, 2016).

2.3. NRF2 and the cellular antioxidant response: friend or foe?

The nuclear factor erythroid 2–related factor 2 (NRF2) is the master regulator of cellular antioxidant responses. It is encoded by erythroid-derived 2-like 2 (NFE2L2) gene and it acts as transcriptional factor (Alam *et al*., 1999). Under "normal" conditions, NRF2 is constantly translated, ubiquitinated and sent to proteasome degradation. In more detail, in the cytoplasm, NRF2 is bound to the dimer formed by Kelch-like ECH-associated protein 1 (KEAP1) which facilitates NRF2 ubiquitination through the binding of the -Cullin-3 (Cul3)/RING box protein1 (RBX1) E3 ubiquitin ligase complex. Consequently, NRF2 is targeted to proteasome degradation (Eggler *et al*., 2009). Following exposure to electrophiles or oxidative stress, KEAP1 undergoes post-translation modification on cysteine residues and its binding to NRF2 is stabilized, so that new translated NRF2 can be accumulated in the cytoplasm and then translocated to the nucleus where it heterodimerizes with sMaf and binds DNA in Antioxidant Responsive Element (ARE). In the nucleus NRF2 fulfill its transactivating function, promoting the translation of cytoprotective genes, such as HO-1, NQO1 and SLC7A11 (Kobayashi & Yamamoto, 2006) (**Fig. 3**). As expected, NRF2 is constitutively active in Keap1 deficient mice, with markedly increased expression of NRF2 target genes relative to wild type controls. Interestingly Keap1 knock-out mice undergoes postnatal lethality due to abnormal keratinization and cornification in the esophagus and forestomach, as ARE contains a subset of genes associated with squamous cell differentiation (Wakabayashi *et al*., 2003).

As already mentioned, NRF2 is a key transcription factor for cellular responses to oxidative stress, activating the transcription of genes that protect the cell from damage caused by free radicals, toxins, and environmental stressors. This protective role is essential for maintaining genome and, in general, cellular integrity (Goodfellow *et al*., 2020; Yagishita et al., 2014), thereby acting as a tumor suppressor. However, in many advanced cancers, NRF2 is chronically hyperactivated, often due to mutations in KEAP1, especially in non-small cell lung cancer (NSCLC) (Scalera *et al*., 2022), which prevents NRF2 degradation. This persistent activation has pro-tumorigenic effects, it confers resistance to oxidative stress and chemotherapeutic drugs, promotes cell proliferation, survival, and progression, supporting uncontrolled growth (Ghorbanhosseini *et al*., 2025; Gong *et al*., 2020; Wang *et al*., 2025).

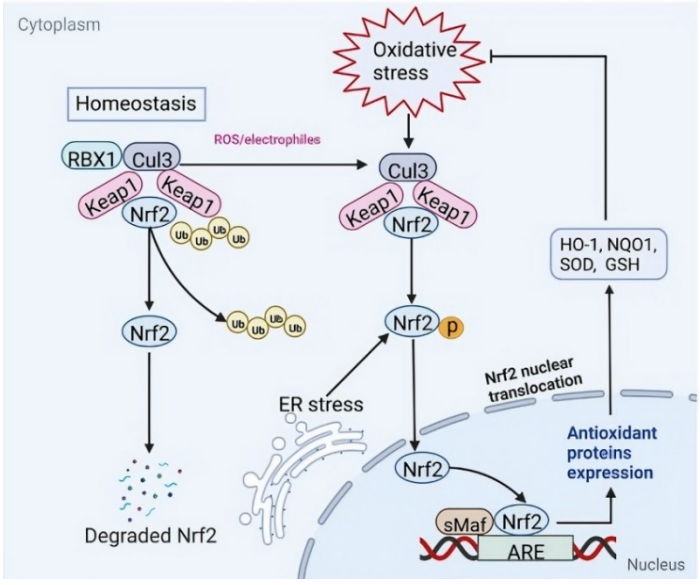

Fig. 3 NRF2/ARE signaling pathways in homeostasis and upon oxidative stress (Wu *et al*., 2022).

2.4. MAPK15 sustains the cellular program for maintaining genome stability

In 1999 Abe *et al*. for the first time described a novel member of the MAPK family, ERK7, in rat. It turned out that ERK7, a protein of 546 amino acids heavy 61 kDa, is widely distributed across different tissues although at low levels (Abe *et al*., 1999). The group described ERK7 as a kinase belonging to the Threonine-Glutamate-Tyrosine (TEY) family, together with ERK1 and ERK2, but, unlike them, no upstream activated MAPKK targeting ERK7 was identified. Interestingly, even nowadays activating proteins of ERK7 are not known and Abe *et al*. (2001) observed that its activation is due to its autophosphorylation on tyrosine and threonine residues within the TEY motif (Abe *et al*., 2001).

Another distinctive characteristic of ERK7 is that it shares with ERK1 and ERK2 approximately 40% of the aminoacid sequence but has a unique C-terminal region required for its activity. In fact, Abe *et al*. (1999) described that the truncated C-terminal ERK7 mutant is auto-phosphorylated less efficiently *in vitro* compared to ERK7 wild-type protein. Moreover, they found out that the C-terminal region is fundamental for ERK7 nuclear localization and for its inhibition of cell growth, while the kinase domain has no influence on these two functions (Abe *et al*., 1999).

In 2002, Abe's laboratory took advantage of rat Erk7 cDNA as a probe to identify proteins characterized by TEY motif in human tissues (Abe *et al*., 2002). They discovered a gene, located on chromosome 8, with a TEY motif but quite different from ERK7 (indeed this new protein shared relatively low aminoacidic sequence similarity with ERK7: 82% of identity in the kinase domain, 53% in the C-terminal region) This new kinase lacked constitutive kinase activity and was not able to phosphorylate c-FOS. For these reasons, they called the new protein ERK8, adding it to the ERK family as a new member, although related to ERK7 (Abe *et al*., 2002). It was showed that ERK8, like ERK7, can autophosphorylate on tyrosine and threonine residues within the TEY motif (Abe *et al*., 2002). Furthermore, they demonstrated that ERK8 mRNA is expressed in different tissue types, particularly in lung and kidney and that the protein is expressed at a very low level and it is activated by a SRC family protein. Moreover, ERK8 activation is induced by serum stimulation but the response is always mediated by SRC family kinases (Abe *et al*., 2002).

In 2006, Klevernic *et al*. clarified some aspects regarding ERK8 phosphorylation, confirming that ERK8 activity is due to its autophosphorylation and specifying that its activity depends more on the phosphorylation of the threonine residue, rather than of the tyrosine one. They also analyzed the myelin basic protein phosphorylated by MAPK15 *in vitro* through mass spectrometry and demonstrated that ERK8 is a proline-directed serine/threonine kinase with a substrate specificity distinct from ERK2 (Klevernic *et al*., 2006). Furthermore, in accordance with Abe's laboratory (Abe *et al*., 2002), they also noted an extremely low activity of ERK8 in mammalian cells and discovered that hydrogen peroxide (H_2O_2) is able to stimulate the phosphorylation of MAPK15, activating the protein, in a very fast manner (about 10 minutes). Ultimately, they noticed that this phosphorylation can be suppressed using indoyl bismaleimide Ro 318220 that acts directly on MAPK15 (Klevernic *et al*., 2006). We can say that in this study Klevernic outlined the first evidence of the MAPK15 involvement in antioxidant response, detailed in the present study.

After these findings, subsequent studies demonstrated that human ERK8 is the homolog of rat ERK7, and the human protein began to be called ERK8 or ERK7 interchangeably. As the use of different names to indicate the same protein in distinct species can be confusing, the use of the MAPK15 name,

recommended by the HUGO Gene Nomenclature Commitee and Protein Knowledgebase of UniProt, is preferable.

MAPK15 is involved in different cellular processes from regulating nuclear receptors (Henrich *et al*., 2003; Rossi *et al*., 2010; Saelzler *et al*., 2006) to ciliogenesis (Piasecki *et al*., 2017). Furthermore, it has been recently established that MAPK15 is involved in tumor development. For example, Iavarone *et al*. (2006) found out that RET/PTC3 and RET/MEN2B, two oncogenic RET mutations often present in thyroid cancers, activate MAPK15, suggesting a role for this kinase in the transforming activity of RET derived oncogenes (Iavarone *et al*., 2006). In 2010, Xu *et al*. demonstrated the tumorigenic role of MAPK15 (Xu *et al*., 2010). They showed that overexpression of MAPK15 in a normal mouse epidermal cell line leads to quicker growth and a more massive colonies formation compared to empty vector-transfected control. On the other hand, many studies reported MAPK15 as a supporting factor of cellular genome stability. In fact, Colecchia et al. (2012), demonstrated that an overexpression of MAPK15 induces autophagy process thanks to the ability of the kinase to directly interact with ATG-8 like proteins inducing their lipidation (Colecchia *et al*., 2012). On the contrary, MAPK15 kinase-dead mutant cannot induce the formation of autophagosomal structures. Furthermore, Groehler and Lannigan (2010) found out that in absence of MAPK15, in cells exposed to ultraviolet-C (UVC), the DNA damage is increased compared to control (Groehler and Lannigan, 2010). Conversely, four hours after treatment, DNA damage is greatly reduced in control cells, but it continues to increase in the MAPK15 knock-down cells, suggesting the importance of MAPK15 for DNA repair mechanisms. They were able to demonstrate that MAPK15 plays this reparative role interacting directly with PCNA, stabilizing the fraction of this protein binding to chromatin. More recently, Franci *et al*., (2022), gave evidence that MAPK15 promotes mitophagy by activating ULK1 dependent phosphorylation of PRKN and facilitating the targeting of damaged mitochondria to autophagosomes and lysosomes (Franci *et al*., 2022). Indeed, they showed that when MAPK15 is depleted from cells, mitochondrial ROS (mROS) increased, causing DNA damage, and the cells lose the ability to eliminate mitochondria after induced damage. But, after MAPK15 overexpression, not only mROS decrease, but also mitochondria colocalized with autophagosome increase indicating that mitophagy is taking place. Since damaged mitochondria overproduce ROS, we can say that mitophagy sustained by MAPK15 reduces oxidative stress, consequently protecting cells from nuclear DNA damage and from aging triggered by persistent DNA damage (Franci *et al*., 2022). Autophagy, mitophagy and DNA repair are fundamental processes for maintaining cellular integrity and genome stability. Indeed, it is well recognized that autophagy and mitophagy are triggered under condition of oxidative stress helping to remove and recycle damaged biomolecules and dysfunctional organelle, thereby helping to reduce oxidative stress and the consequent genomic instability (Filomeni *et al*., 2015).

In conclusion, several studies have demonstrated the role of MAPK15 in sustaining cellular program for genome integrity maintenance. In the present research we elucidated a novel MAPK15 dependent mechanism for cells for managing oxidative stress, indagating its regulation upon NRF2 protein, the master regulator of antioxidant responses.

This thesis is based on the research of Franci, L., **Vallini, G.**, Bertolino, F. M., Cicaloni, V., Inzalaco, G., Cicogni, M., Tinti, L., Calabrese, L., Barone, V., Salvini, L., Rubegni, P., Galvagni, F., & Chiariello, M. (2024). MAPK15 controls cellular responses to oxidative stress by regulating NRF2 activity and expression of its downstream target genes. *Redox Biology*, *72*, 103131.

3. Material and methods

3.1. Cell culture

HeLa and 393T cell lines were cultured in DMEM supplemented with 10% fetal bovine serum (FBS), 2mM L-glutamine and 100 units/ml of penicillin-streptomycin. A549, NCI–H358 and NCI-H460 cells were maintained in RPMI 1640 Medium supplemented with 10% FBS, 2 mM L-glutamine and 100 units/ml penicillin-streptomycin. NIH3T3 (CRL-1658) cells were maintained in DMEM supplemented with 10% calf serum, 2 mM L-glutamine and 100 units/ml penicillin-streptomycin. Primary human airway epithelial cells (hAEC) were maintained in hAEC medium (Epithelix).
All cells were maintained at 37°C in an atmosphere of 5% CO_2/air.

3.2. Expression vectors and transfections methods

The HA-tagged form of MAPK15 (pCEFL-HA-MAPK15) was generated by cloning the corresponding cDNA, kindly donated by M. Abe (Abe *et al*., 2002), in the pCEFL-HA vector. The kinase dead mutant MAPK15 D155A (MAPK15 KD) cDNA was a generous gift from Philip Cohen (University of Dundee) and then subcloned into pCEFL-HA plasmid, as described in one of our previous works (Colecchia *et al*., 2012). pGL4.37 [luc2P/ARE/Hygro] (Promega, 9PIE364), pLenti-NRF2-MYC-FLAG-tagged (Origene, RC204140L1) were purchased from indicated distributors. Vectors used to stably silence NIH3T3 mouse cells were: shSCR, scrambled control and shMAPK15 (GCAATGGAATCTCTGCACG). The S40A point mutation in pLenti-NRF2_Myc-FLAG was introduced using the QuickChange XL Site-Directed Mutagenesis kit (Agilent, Santa Clara, CA), according to the manufacturer's instructions, with the following oligonucleotides: 5'-GTCGAGAAGTATTTGACTTCGCTCAGCGACGGAAAGAGTAT-3' and 5'-ATACTCTTTCCGTCGCTGAGCGAAGTCAAATACTTCTCGAC-3'. The expression of NRF2 protein in bacteria was obtained used pPROEX-HTc-Flag3-Nrf2, donating by Yue Xiong (Addgene plasmid #21553). For DNA plasmid transfection, 3×10^5 cells were seeded in 6-well cell culture plates. 24 h after seeding, cells were transfected with 1 µg of each expression vector diluted in 200 µl of OptiMEM medium (Gibco) and Lipofectamine LTX (Life Technologies), 5 µl per µg of DNA. After 24 h from transfection, cells were lysed according to the target of each downstream experiment, with NP-40 buffer for protein extraction (see paragraph 3.5) or QIAzol Lysis Reagent (Qiagen) for nucleic acids (see paragraph 3.7).

3.3. Small-interfering RNA (siRNA) and transfection methods

In the same manner for all cell lines mentioned in the paragraph above, 1×10^5 cells were seeded in 6-well cell culture plates and, after 24 h, transfected using MAPK15-specific siRNA (5'-TTGCTTGGAGGCTACTCCCAA-3') or non-silencing control siRNA (scramble, 5'-AATTCTCCGAACGTGTCACGT-3'), diluted in 200 µl of OptimMEM medium (Gibco) and a volume of transfection reagent dependent on type of cell line. siRNAs were used at final concentration of 100 nM. The used transfection reagents were HiPerfect (Qiagen) for HeLa cells (7.5 µl) and RNAiMAX (Life Technologies) for hAEC (7.5 µl), NCI–H358 (6.5 µl), 293T (6 µl), A549 (6 µl) and NCI-H460 (6 µl). After 72 h from transfection, cells were lysed according to the target of each downstream experiment, with NP-40 buffer for protein extraction (see paragraph 3.5) or QIAzol Lysis

Reagent (Qiagen) for nucleic acids (see paragraph 3.7). Where indicated, co-transfection with pLenti-NRF2-MYC-FLAG-tagged or pGL4.37 [luc2P/ARE/Hygro] were performed 24 or 48 h after siRNA transfection, respectively.

3.4. Cell treatments

Cells, transfected with siSCR or siMAPK15 and/or with different expression vectors described before (see paragraphs 3.2 and 3.3), were treated with different reagents described in **Table 2**.

Reagent	**Supplier and catalog number**
Carbonylcyanide-4-(trifluoromethoxy)-phenylhydrazone (FCCP)	Abcam (370-86-5)
Cycloheximide (CHX)	Merk (01810)
Sorafenib	MedChemExpress (284461-73-0)
TMCB	Santa Cruz (sc-361383)
Sulforaphane (SFN)	Santa Cruz (sc-361383)
Dimethyl fumarate (DMF)	Santa Cruz (sc-239774)
GO6983	Med Chem Express (HY-13689)
12-O-Tetradecanoyl-phorbol-13-acetate (TPA)	Med Chem Express (HY-18739)
Ro-318220	ChemCruz (sc-200619)
Condensed smoke extract (CSE)	See paragraph 3.9.
H_2O_2	-

Table 2 List of reagents used for cell treatment

3.5. Protein extraction and Western blot assay

Cells were lysed with 1% NP-40 buffer (50 mM TRIS-HCl pH = 8.0, 150 mM NaCl, 0.5% sodium deoxycholate, 0.1% SDS, 1% NP-40) with the addition of protease inhibitors (complete Protease Inhibitor cocktail, EDTA-free; Roche Diagnostics) and phosphatase inhibitors (2 mM NaF, 2 mM Na3VO4; Sigma Aldrich). Lysates were incubated in ice for 15 min and centrifugated at 4°C at 16.000g. Pellet was discarded and the supernatant conserved for downstream assay. The proteins were quantified through Bradford colorimetric assay and between 15 to 30 mg of proteins were used for Western blot (WB) experiment. Each proteic sample was mixed with Laemmli Loading Buffer 5X (250 mM Tris-HCl pH 6.8, 10% SDS, 50% glycerol, bromophenol blue) and heated for 5 min at 95°C. Lysates were loaded on SDS-PAGE polyacrylamide gel, transferred to Immobilon-P PVDF

membrane (Merck Millipore), probed with appropriate primary and secondary antibodies, and revealed by enhanced chemiluminescence detection (ECL Plus; GE Healthcare). Densitometric analysis of WB was performed with NIH Image J (National Institutes of Health).

3.6. Co-immunoprecipitation

With transfection method described in paragraph 3.2., HA-MAPK15 plasmid was co-transfected with NRF2-MYC-FLAG plasmid in 293T cells. After 24 hours, cells were lysed with NP-40 lysis buffer and centrifugate to collect the supernatant containing proteins. The primary antibody anti-HA was equilibrated in lysis buffer. 2 mg of proteins were resuspended in 290 µl of lysis buffer and 10 µl of primary antibody anti-HA and incubated for 2 h at 4°C rocking. Meanwhile, protein G Mag Sepharose™ Xtra beads (28-9670-66, Cytiva) were equilibrated in lysis buffer for 30 min at 4°C rocking. After incubation, 50 µl of magnetic beads were added to sample and incubated for 1 h at 4°C rocking. After incubation, sample was placed in magnetic rack to separate beads from supernatant. Beads were washed with washing buffer (PBS with 1% of NP-40) several times and attached proteins were eluted using 2X Laemmli buffer. The Western blot analysis was performed on eluted proteins using anti-NRF2 antibody.

3.7. Immunofluorescence

1×10^4 cells were seeded in 12-well cell culture plates and transfected with each siRNA and DNA plasmid as described above. After 72 h, cells were washed with PBS, fixed with ice-cold methanol for 10min, permeabilized with 0.2% Triton X-100 solution for 20min and then blocked for 20min with 2.5% BSA diluted in PBS. Next, cells were incubated with primary antibodies for 30min, washed three times with PBS, and then incubated with appropriate Alexa Fluor 488-conjugated (Invitrogen, A21202) or Alexa Fluor 555-conjugated (Invitrogen, A31570) secondary antibodies. Nuclei were stained with 1.5 µM 4′,6-diamidino-2-phenylindole (DAPI) (VWR) in PBS for 5 min. Coverslips were mounted in fluorescence mounting medium (Dako, S3023). Samples were visualized on a TSC SP5 confocal microscope (Leica, 5100000750) installed on an inverted LEICA DMI 6000CS (10741320) microscope using an oil immersion PlanApo 40 × 1.25 NA. Images were acquired using the LAS AF acquisition software (Leica). Fluorescence intensity was analyzed using the Quantitation Module of Volocity software (PerkinElmer Life Science, I40250).

3.8. mRNA extraction and real-time quantitative PCR

To quantify gene expression, cells were lysed with 1 ml of QIAzol Lysis Reagent (Qiagen). Removal of contaminating genomic DNA and reverse transcription were performed with the QuantiTect Reverse Transcription Kit (Qiagen). The following primer pairs were used:

mouse primers

m_HPRT_Forw 5'-GGCCCTCTGTGTGCTCAAG-3';
m_HPRT_Rev 5'- CTGATAAAATCTACAGTCATAGGAATGGA-3';

m_MAPK15_Forw 5'- GCCCGGACGCAATCGCTCAA-3';
m_MAPK15_Rev 5'- GGGCTACGCGGAGGTTTGGG-3';

human primers

h_MAPK15_Forw 5'-TGGCCAGCGTACAACAGGT-3';
h_MAPK15_Rev 5'-CAGTCCCGTAGGCTTGGGAGTA-3';

h_MAPK1_Forw 5'-GCCCATCTTTCCAGGGAAGCATTA-3';
h_MAPK1_Rev AGAGCTTTGGAGTCAGCATTTGGG-3';

h_HO-1_Forw 5'-CAACATCCAGCTCTTGAGG-3';
h_HO-1_Rev 5'-GGCAGAATCTTGCACTTTG-3';

h_NQO1_Forw 5'-GAAGAGCACTGATCGTACTGGC-3';
h_NQO1_Rev 5'-GGGTCCTTCAGTTTACCTGTGAT-3';

h_MGST1_Forw 5'-TCGTGACAAAGCAAATTGTCTGG-3';
h_MGST1_Rev 5'-CCATTACCTGGGTGAGGTCAA-3';

h_NRF2_Forw 5'-CAGCGACGGAAAGAGTATGA-3';
h_NRF2_Rev 5'-TGGGCAACCTGGGAGTAG-3';

h_GCLM_Forw 5'-GGAACCTGCTGAACTGGGG-3';
h_GCLM_Rev 5'-CCCTGACCAAATCTGGGTTGA-3';

h_GCLC_Forw 5'-GTTCTTGAAACTCTGCAAGAGAAG-3';
h_GCLC_Rev 5'-CCTTCAATCATGTAACTCC-3';

h_SLC7A11_Forw 5'-TGCCCAGATATGCATCGTCC-3';
h_SLC7A11_Rev 5'-GGGCAGATTGCCAAGATCTCA-3';

h_AKR1B10_- Forw 5'-CAGCAACAGAGAGCAGGACG-3';
h_AKR1B10_Rev 5'-TGCTGACGATGAACAGGTCC-3'.

3.9. ROS quantification

3×10^5 cells were seeded in 6-well cell culture plates and transfected with DNA plasmid or seeded at minor density (1×10^5 cells) for siRNA-DNA plasmid co-transfection. After 24 h or 72 h, respectively, ROS quantification was performed incubating cells with 0.5 μM or 1 μM of CM-H2DCFDA (Invitrogen, C6827) for 30 min in medium without serum according to the manufacturer's protocol. Cells were resuspended in PBS and acquired on a FACSCanto II flow cytometer (BD Biosciences). Data was analyzed with FlowJo software.

3.10. Condensed smoke extract preparation

Condensed smoke extract (CSE) was obtained from Marlboro Red cigarettes (Phillip Morris, 13 mg/cig tar and 0.9 mg/cig nicotine). CSE was produced by blowing the smoke from 10 cigarettes into 100 ml of PBS at a rate of 1 cigarette/min. This was considered as 100% CSE. The 100% CSE was passed through the 0.22 μm filter, aliquoted, and stored at −80°C.

3.11. Antibodies

The following primary antibodies were used for WB and confocal microscopy experiments: anti-MAPK15 (Invitrogen PA5-75930), anti-HA (Covance, MMS-101R) anti-MAPK1 (Santa Cruz, sc-

154), anti-NRF2 (Cell Signaling, 12721), anti-phospho-NRF2_Ser40 (Abcam, ab180844), anti-IKBα (Santa Cruz, sc-371), anti-Flag (Sigma, F1804) anti-γH2A.X (Cell Signaling, 9718), anti-53BP1 (Novus, NB100-304), anti-NQO1 (Santa Cruz, sc-207495A), anti–HO–1 (Santa Cruz, sc-136960 for mouse samples and Genetex GTX101147 for human samples), anti-phospho-NRF2_Ser40 (Invitrogen, PA567520), anti-SLC7A11 (Cell Signaling, D2M7A); Anti-Phospho-PKC (pan) (βII Ser660) (Cell Signaling, 9371); anti-PKC (A-3) (Santa Cruz, sc-17769); anti-Myc (Cell Signaling, 2276); anti-Phospho-Ser/Thr-Pro (Upstate, 05–368). The following secondary antibodies were used for WB experiments: anti-mouse (Jackson ImmunoResearch, 115-036-003) and anti-rabbit (Jackson ImmunoResearch, 111-036-003) HRP-conjugated IgGs.

3.12. Luciferase assays

Cells were transfected with 5 ng of the ARE-luciferase reporter vector and 1 µg of different expression vectors. 24 h after transfection, cells were treated with FCCP or CSE for the indicated time and concentration (see paragraph 3.4), then lysed in Passive Lysis Buffer (Promega) and luciferase activity in the cellular lysates was assessed on a Glomax 20/20 luminometer (Promega) using the Luciferase Assay System (Promega). Results were normalized for transfection efficiency by using a GFP coding vector (1 µg). All samples were read in triplicate.

3.13. Samples preparation, LC-MS/MS and bioinformatics analysis

In collaboration with Dr. Cicaloni LC-MS/MS and bioinformatics analysis were conducted. A solution of 2% sodium deoxycholate (SDC)/100 mM ammonium bicarbonate was used to lyse the samples. The cell lysates were alkylated in the dark with 10 mM Iodoacetamide at room temperature for 30 min after being reduced with 5 mM tris(2-carboxyethyl)phosphine (TCEP) at 60 °C for 30 min. Bicinchoninic acid (BCA) assay was used for protein quantification. 60 µg of proteins, for each sample, were processed by adding trypsin using an enzyme-to-protein ratio of 1:40 and incubated at 37 °C overnight. After digestion, all reaction mixtures were acidified with 1% formic acid to inhibit any residual enzyme activity and precipitate the SDC (Lin *et al*., 2008; Zhou *et al*., 2006). Digested samples were desalted with OASIS cartridges (Waters), brought to dryness, and reconstituted in 0.1% formic acid in water/acetonitrile (97/3, v/v). QExactive Plus Orbitrap mass spectrometer (Thermo Fischer Scientific) was used to conduct LC-MS/MS analysis. The Acquity UPLC™ peptide CSH C18 column, 1 mm × 100 mm, 1,7 µm, 130 (Waters) was used for the peptide separation at 50 °C with a flow rate of 100 µl/min. The mobile phases A and B used for the analysis were 0.1% formic acid in water and 0.1% formic acid in acetonitrile respectively. These experiments were performed using a data dependent analysis (DDA) setting to select the "top twelve" most-abundant ions for MS/MS analysis. Protein identification was performed using Proteome Discover 2.1 (Thermo Scientific) and Sequest algorithm by using Mus musculus database from UniprotKB (organism ID 10090). Moreover, the default peak-picking settings were used to process the raw MS files in MaxQuant (version 1.6.1.0) (Cox & Mann, 2008) and its integrated search engine Andromeda (Cox *et al*., 2011). Protein identification and label free quantification (LFQ) by MaxQuant/Andromeda was based on at least one unique peptide with a minimum length of seven amino acids and a false discovery rate of 0.01 applied to both peptide and protein level. By default, the alignment time window size was 20 min, and the match time window size was 0.7 min. The cutoff for peptide and protein identifications was set at False Discovery Rate (FDR) of 0.01. The runs were automatically

aligned by MaxQuant. The peak intensities across the whole series of measurements were compared using the free software Perseus (version 1.6.1.1) to analyze MaxQuant result files and provide quantitative information for all the peptides in the sample. Proteins identified from the reverse sequence database or based on a single modified peptide, as well as contaminant proteins identified from the contaminant sequence database, were filtered out. The LFQ intensities of proteins from the MaxQuant analysis were imported and transformed to logarithmic scale with base two. The protein quantification and calculation of statistical significance was carried out using two-way Student-t test and error correction (p value < 0.05) with the method of Benjamini–Hochberg. For further visualization, Principal Component Analysis (PCA) were performed to investigate underlying differences between samples and replicates in quantitative proteomics results. Moreover, volcano plots were used to show a summary distribution of differentially expressed proteins between samples. The volcano plot is an easy-to-interpret scatter plot that arranges values along dimensions of statistical (log10 p-value) significance. The proteins located on the upper left region and the upper right region are differentially expressed.

3.14. Nuclear-cytoplasmic fractionation

1×10^5 cells were seeded in 6-well cell culture plates and, after 24h, transfected using MAPK15-specific siRNA or non-silencing control siRNA. After 72 h, cells were treated with 300 nM H_2O_2 for 1 h or CSE 1% or 2.5% for 4 h and then subjected to fractionation. Cytoplasmic and nuclear fractions were obtained by NE-PER Kit (Thermo Scientific, 78833), according to the manufacturer's protocol.

3.15. Kinase assay

Purified recombinant protein of full length MAPK15 was purchased from Origene (Cat. N. TP761629). The BL21 strain of Escherichia coli (E. coli) was transformed with the pPROEX-HTc vector encoding for the full-length form of the NRF2 protein, tagged with 6xHis and Flag3x. Bacteria were lysed in lysis buffer (50 mM NaH2PO4 pH 8.0, 300 mM NaCl, 10 mM Imidazole, 0.05% Tween and 0.2 mg/ml of lysozyme) and incubated for 30 min. Bacterial lysate was centrifugated (15 min at 7,500 x g) and the supernatant incubated for 1 h with His mag Sepharose™ Ni magnetic beads (Cytiva, 29104065). After several washes in washing buffer (50 mM NaH2PO4 pH 8.0, 300 mM NaCl, 20 mM Imidazole, 0.05% Tween) the beads were resuspended in elution buffer (50 mM NaH2PO4 pH 8.0, 300 mM NaCl, 250 mM Imidazole, 0.05% Tween). After an incubation of 5 min, the beads were centrifugates (1 min at 5,000 x g) and the eluate, containing the recombinant protein, was taken for downstream assay. MAPK15 purified protein (50 ng/sample) was incubated 30 min at 30°C in kinase buffer [25 mM HEPES (pH = 7.6), 0.1 mM Na3VO4, 20 mM β-glycerophosphate, 2 mM DTT, 20 mM MgCl2, 25 µM ATP] with 2.5 µg/sample of the NRF2 protein. Reaction was stopped adding Laemmli buffer and resolved by SDS-PAGE followed by WB analysis or followed by peptide mass fingerprint (PMF) and phosphorylation detection. Kinase activity was estimated by densitometric analysis of WBs, performed with NIH Image J software (National Institutes of Health), or by mass spectrometry, as described below (see paragraph 3.15). For WB Coomassie staining [ProBlue Safe Stain (Giotto Biotech, G00PB002)] and WB analysis of kinase reactions were used as loading controls.

3.16. Peptide mass fingerprint (PMF) and phosphorylation investigation

Purified proteins from the kinase reaction samples were subjected to overnight in-solution digestion by trypsin (Promega) at 37°C, after reduction with dithiothreitol (DTT, final concentration 10 mM, Merck Group) and alkylation with iodoacetamide (IAA, final concentration 25 mM, Merck Group) [30]. The resulting peptides were brought to dryness and reconstituted in 0.1% formic acid in water. LC-MS/MS analyses were performed using Q-Exactive HF-X Orbitrap mass spectrometer (Thermo Scientific). The peptide separation was carried out at 35 ◦C using a PepMap RSLC C18 column, 75 µm × 15 cm, 2 µm, 100 Å (Thermo Fisher) at a flow rate of 300 nl/min. The mobile phases A and B used for the analysis were 0.1% formic acid in water and 0.1% formic acid in 80% acetonitrile, respectively. The gradient started with 5% of B and then it was increased to 90% in 60 min. The data were elaborated using BioPharma Finder 2.0 (Application Note 21682, Thermo Fisher) comparing the list of peaks obtained "in silico" simulating protein digestion of the expected aminoacidic sequence (retrieved from UniProtKB, accession code: Q16236) and the experimental data. Phosphorylation was set up as post-translational modification (PTMs) in addition to carbamidomethylation and methionine/tryptophan-oxidation.

3.17. Statistical analysis

Significance (p value) was assessed by pairwise Student's t-test, using GraphPad Prism8 software. Asterisks were attributed as follows: *$p < 0.05$, **$p < 0.01$, ***$p < 0.001$.

4. Results

4.1. Proteomic analysis reveals MAPK15 as a potential regulator of NRF2 target genes

We started performing proteomic analysis, in collaboration with Dr. Cicaloni, on NIH3T3 fibroblast cell line isolated from a mouse embryo interfered for MAPK15 thanks to short hairpin (sh) RNA approach (shMAPK15), comparing to scrambled/control transfected cells (shSCR) (**Fig. 4A**). 1735 and 1706 high-confidence proteins for shMAPK15 and for shSCR, respectively, were examined.
Specifically, 2011 quantifiable unique proteins with association to a known Mus musculus gene were found. Next, proteomics datasets were further categorized and examined with various statistical tools to provide a high-level understanding of the similarities and differences between shSCR and shMAPK15 samples. Principal Component Analysis (PCA) was employed to explore the sample separation and cluster. The first two main PCA components explained 46.0% and 17.1%, for a total of 63.1%, of the variation (**Fig. 4B**) confirming a sizeable percentage. All triplicates of shSCR and shMAPK15 samples included in the analysis appeared to cluster in two distinct groups, reinforcing the evidence of a clear different proteomic dataset between shSCR and shMAPK15 (**Fig. 4B**).
Next, we identified 1430 proteins present in both shSCR and shMAPK15 cells (the "overlap index", based on Jaccard similarity coefficient, is 0.71), 305 proteins present exclusively in the shSCR samples and 276 only in shMAPK15 samples. Among the 305 proteins present in shSCR samples and absent in shMAPK15 ones, we observed many NRF2 target genes, as Heme-oxygenase 1 (HO-1), Metallothionein-2 (MT2), Microsomal glutathione S-transferase 1 (MGST1), Superoxide dismutase 3 (SOD3) and UDP-glucuronosyltransferase 1–6 (UGT1A6) (**Fig. 4C**). We even analyzed the proteins subset shared between shSCR and shMAPK15 cells and, among them, other NRF2 target genes, such as NAD(P)H quinone dehydrogenase (NQO1) and Epoxide hydrolase 1 (EPHX1), are upregulated in shSCR compared to shMAPK15 samples, suggesting that their expression is impaired when MAPK15 is depleted. In the volcano plot, proteins differentially expressed are located on the upper left region and on the upper right region (S0 = 1, FDR<0.05) (**Fig. 4D**).
To validate proteomic analysis, we performed Western blot (WB) in same cells described above, and in line with the bioinformatics result, we confirmed that NRF2 target genes are effectively downregulated when cells lose MAPK15 expression, suggesting role of MAPK15 in controlling NRF2 activity (**Fig. 4E**). Indeed, we found that NRF2 is strongly downregulated when MAPK15 is silenced NIH3T3 cells (**Fig. 4F**). Taken together, these data suggest that MAPK15 regulates level of NRF2 inducible proteins acting upstream of them, probably at NRF2 level.

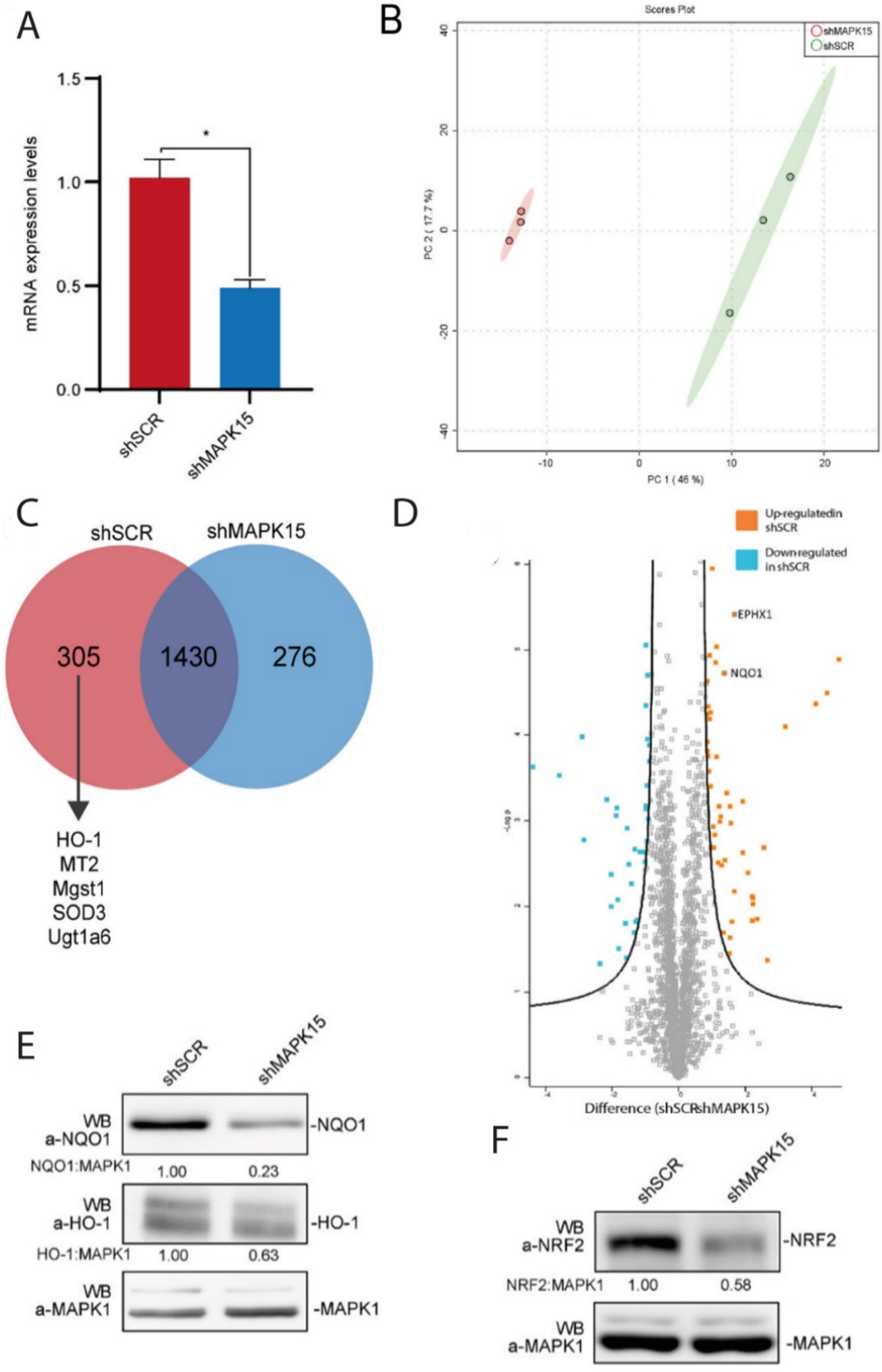

Fig. 4 (**A**) Relative mRNA levels of MAPK15 in NIH3T3 cells interfered for MAPK15 (shMAPK15) compared to control (shSCR) (**B**). Principal Component Analysis (PCA)-biplot for shSCR and shMAPK15 samples. (**C**) Venn diagram shows subsets of proteins uniquely expressed in shSCR, in shMAPK15 samples and the one shared by these two. (**D**) Volcano plot shows the upregulated and the downregulated proteins of shSCR sample compared to shMAPK15. (**E-F**) One

representative WB experiment of three of lysates of NIH3T3 cells interfered for MAPK15 (shMAPK15) compared to control (shSCR).

4.2. Endogenous MAPK15 regulates NRF2 level and its transcriptional activity

To further investigate how MAPK15 could control NRF2 activity, we performed a luciferase assay, taking advantage from plasmid contain a firefly luciferase gene driven by Antioxidant Responsive Element (ARE) located upstream of the minimal TATA promoter, so we could observe the transcriptional activity of NRF2. To address this, we silenced MAPK15 in HeLa cells using a small interfering RNA (siRNA) approach (**Fig. 5A-B**) and we found out that NRF2 transcriptional activity is intensely attenuated in comparison with control (siSCR) both at basal level and under stimulation (**Fig. 6A-B**). Indeed, NRF2 transcriptional activity is strongly induced after cyanide 4 (trifluoromethoxy)phenylhydrazone) (FCCP), a chemical compound commonly used to induce oxidative stress acting disrupting mitochondrial membrane potential (Fogo *et al*., 2024; Han *et al*., 2009), or H_2O_2, a non-radical ROS, treatment in siSCR cells, but in MAPK15 downregulated sample treated with FCCP or H_2O_2 the transcriptional activity of NRF2 undergoes a huge decrement, suggesting that cells are not capable of activating NRF2-dependent antioxidative defense after an insult (**Fig. 6A-B**).
To evaluate if also NRF2 target genes are effectively downregulated after MAPK15 depletion, we performed quantitative real-time PCR on HeLa treated with FCCP, and H_2O_2. We chose HO-1, NQO1 and SLC7A11 as representative NRF2 target genes. In non-silenced cells (siSCR), the expression of all three genes increases in a clear manner after FCCP and H_2O_2 insults, but when MAPK15 is silenced, there is a strong decrement of gene expression in treated conditions (**Fig. 6C-D**).
Of notice, we even evaluated the NRF2 mRNA level at basal condition in HeLa and 293T cells and, as we expected, knowing the NRF2 ability to bind its own promoter (Kwak *et al*., 2002), we found that NRF2 gene transcription is significantly decreased (**Fig. 7A-B**).

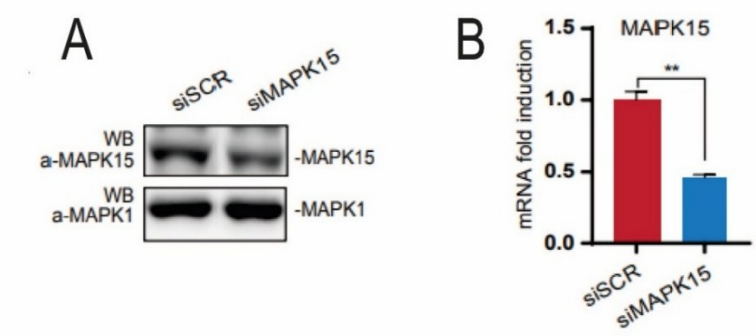

Fig. 5 (**A**) WB experiment of HeLa cells downregulated for MAPK15 (siMAPK15) compared to control (siSCR). (**B**) Relative mRNA levels of MAPK15 in HeLa cells downregulated for MAPK15 (siMAPK15) compared to control (siSCR). All real-time quantitative PCR results represent the average ± S.D. of three independent experiments.

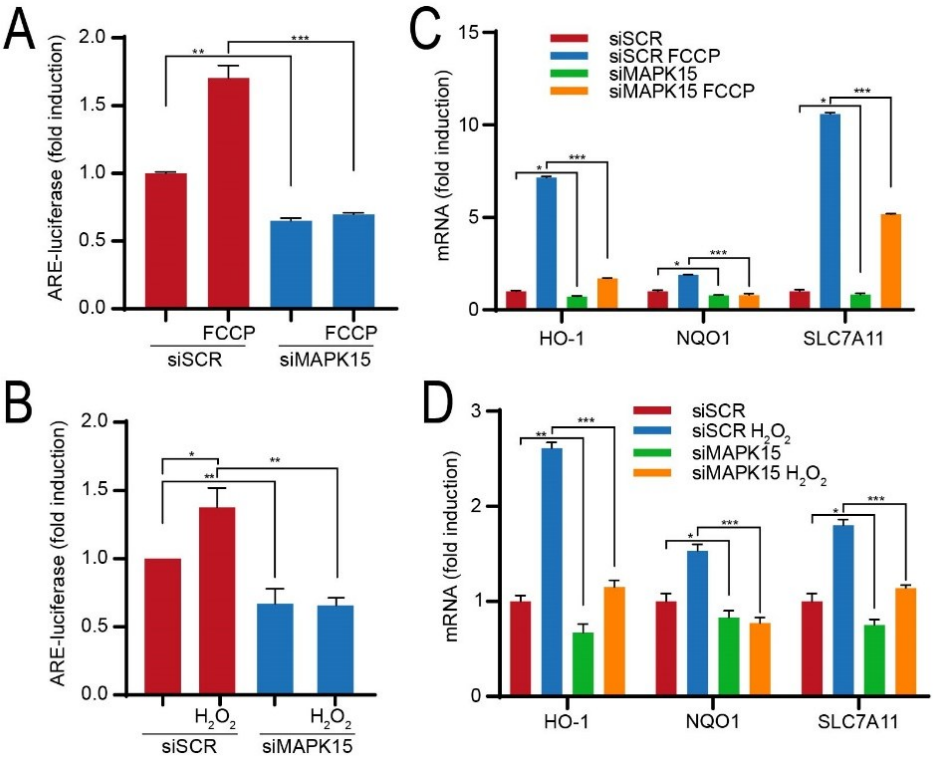

Fig. 6 (**A**) Luciferase assay of HeLa cells downregulated for MAPK15 (siMAPK15) compared to control (siSCR), transfected with ARE luciferase report vector and treated with vehicle or FCCP (30 μM for 6 h). All luciferase results represent the average ± S.D. of three independent experiments. (**B**) Same as in (**A**) but cells were treated with vehicle or H_2O_2 (300 μM for 10 minutes – harvested after 1 h). (**C**) Relative mRNA levels of indicated genes of HeLa cells downregulated for MAPK15 (siMAPK15) compared to control (siSCR) treated with FCCP (30 μM for 6 h). All real-time quantitative PCR results represent the average ± S.D. of three independent experiments. (**D**) Same as in (**C**) but cells were treated with H_2O_2 (300 μM for 2 h).

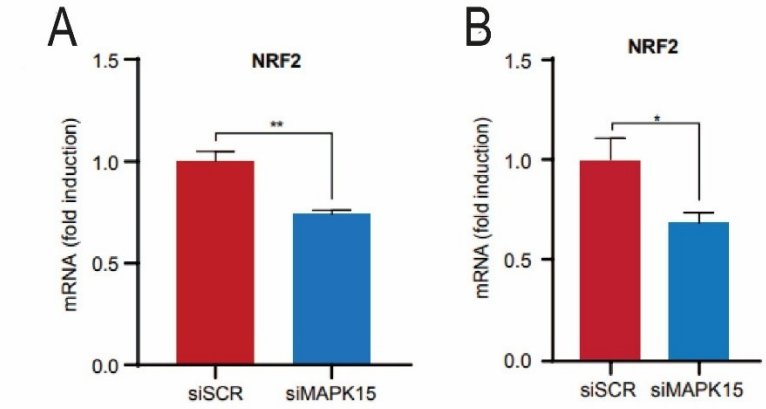

Fig. 7 (**A**) Relative mRNA levels of NRF2 gene in HeLa cells downregulated for MAPK15 (siMAPK15) compared to control (siSCR). All real-time quantitative PCR results represent the average ± S.D. of three independent experiments. (**B**) Same as in (**A**) but experiment was performed in 293T cells.

Even in untreated conditions the decrement of HO-1, NQO1 and SLC7A11 is significant, but less evident. Accordingly, MAPK15 depletion even affects NRF2 protein level that is slightly reduced in siMAPK15 cells in comparison to siSCR ones, but its diminution became much more evident under stimulated conditions (**Fig. 8A-B**).

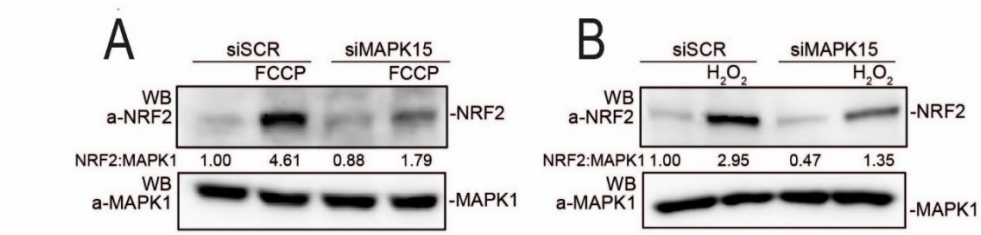

Fig. 8 (**A**) One representative WB experiment of three of lysates of HeLa cells downregulated for MAPK15 (siMAPK15) compared to control (siSCR) treated with FCCP (30 μM for 6 h). (**B**) Same as in (**A**) but cells were treated with H_2O_2 (300 μM for 30 min).

Not only at mRNA level, but also at protein level HO-1, NQO1 and SLC7A11 are downregulated in both untreated and treated (with FCCP and H_2O_2) cells after MAPK15 depletion, as demonstrated by WB experiments (**Fig. 9A-B**).

As a complementary approach, we overexpressed MAPK15 in HeLa cells, demonstrating the strong increment of NRF2 after MAPK15 plasmid transfection compared to cells transfected with empty vector, markedly after oxidative insults with FCCP and H_2O_2 (**Fig. 9C-D**).

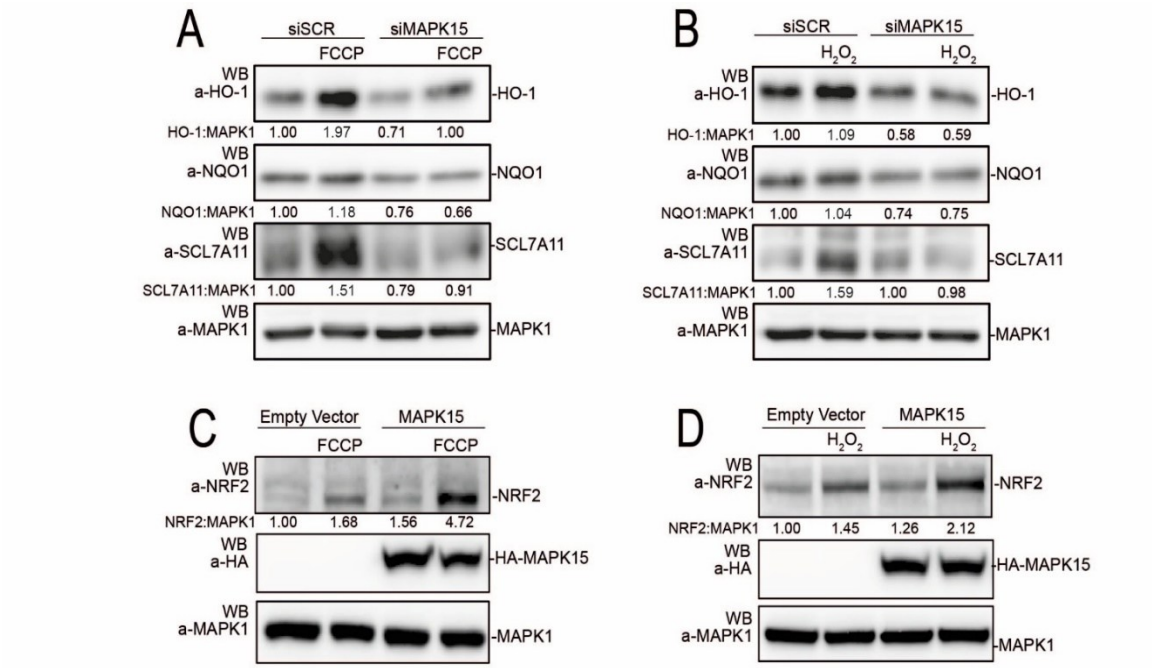

Fig. 9 (**A**) One representative WB experiment of three of lysates of HeLa cells downregulated for MAPK15 (siMAPK15) compared to control (siSCR) treated with FCCP (30 μM for 6 h). (**B**) Same as in (**A**) but cells were treated with H_2O_2 (300 μM for 2 h). **(C**) One representative WB experiment of three of lysates of HeLa cells transfected with MAPK15 plasmid compared to transfected control with empty vector treated with FCCP (**D**) Same as in (**C**), but cells were treated with H_2O_2 (300 μM for 30 min).

Ultimately, we conduct quantitative PCR on NRF2 target genes after stimulating HeLa cells with sulforaphane (SFN) and dimethyl fumarate (DMF), chemical compounds able to activate NRF2 pathway without directly generate ROS (**Fig. 10A-B**).

All data considered, we can conclude that endogenous MAPK15 regulates antioxidant response through NRF2 activity, and its regulation is not only strictly correlated to presence of ROS.

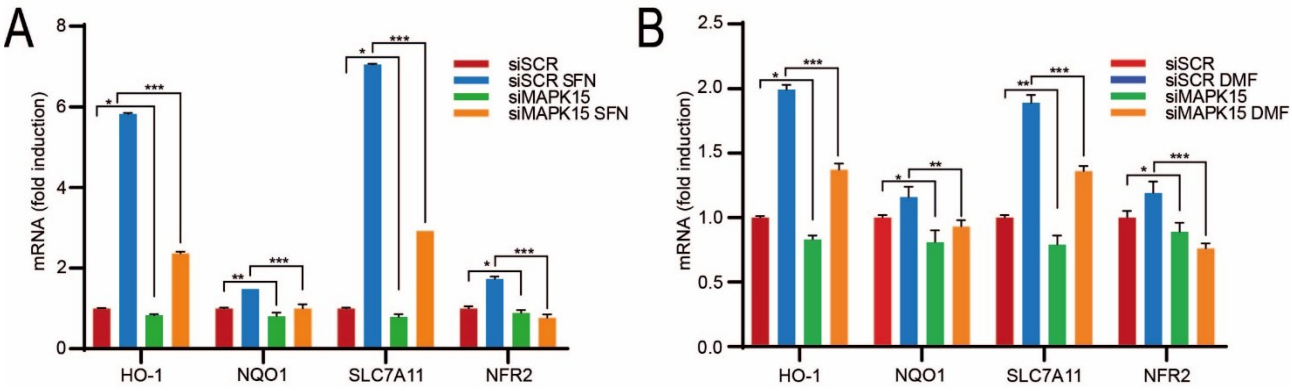

Fig. 10 (**A**) Relative mRNA levels of indicated genes of HeLa cells downregulated for MAPK15 (siMAPK15) compared to control (siSCR) and treated with SFN (10 μM for 6 h). All real-time quantitative PCR results represent the average ± S.D. of three independent experiments. (**B**) Same as in (**A**) but cells were treated with DMF (5 μM for 3 h).

4.3. MAPK15 phosphorylates NRF2 on Thr395-Thr425 and Thr493 residues

As we demonstrated that endogenous MAPK15 regulates NRF2 level (both protein and mRNA level) and its transcriptional activity, we wondered whether MAPK15 regulates NRF2 acting directly or indirectly on this protein. So, we performed a co-immunoprecipitation, co-transfecting 293T cells with NRF2 MYC-FLAG tagged and MAPK15 WT HA-tagged or empty vector. The protein lysate was incubated with anti-HA antibody and immunoprecipitated. The consequent WB assay revealed that MAPK15 co-immunoprecipitates with NRF2 (**Fig. 11**).

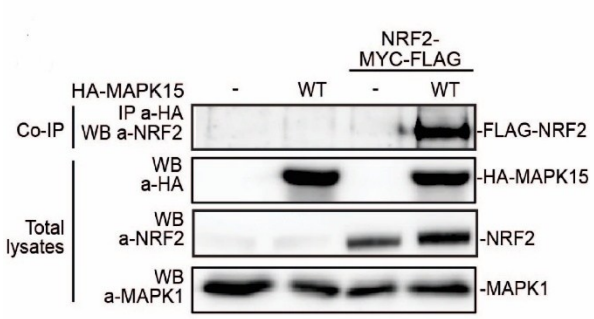

Fig. 11 One representative WB experiment of three of lysates of 293T cells co-transfected with NRF2-MYC-FLAG and HA-MAPK15 or empty vector plasmid and immunoprecipitated with anti-HA antibody. Total lysates were even analyzed.

In vitro kinase assay was performed using recombinant NRF2 and MAPK15 WT purified from bacteria. Samples were analyzed by SDS-PAGE and WB with anti–phospho-serine/threonine-proline antibodies. We found out that MAPK15 directly phosphorylates NRF2 in this protein site (**Fig. 12**).

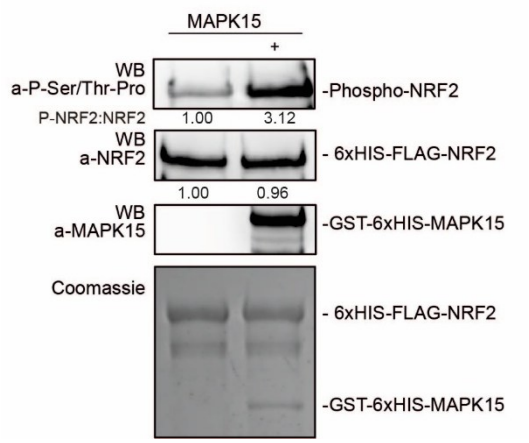

Fig. 12 WB experiment of kinase assay performed between NRF2 and MAPK15 recombinant proteins.

Furthermore, we confirmed these data by performing mass spectrometry analysis on NRF2 protein derived from the kinase assay. In presence of MAPK15, nine NRF2 phosphorylation sites were identified but only three proline-directed threonine phosphorylation sites were found. Specifically, Thr439 and Thr425 were identified even in absence of MAPK15, but they showed different amounts (MS areas) between the control and the MAPK15-containing kinase reactions, while Thr395 was detected only in presence of MAPK15. No proline-directed serine phosphorylation site has been detected. In conclusion, this analysis showed that MAPK15 directly phosphorylates NRF2 in three threonine residues followed by proline, Thr395-Thr425 and Thr439. (**Fig. 13A-B**).

A

	Peptide Sequence	Modification	Site	Delta (ppm)	RT
NRF2+MAPK15	TPVHSSGDMVQPLSPSQGQSTHVHDAQCENTPEK	Phosphorylation	T416	0	31,51
	TPVHSSGDMVQPLSPSQGQSTHVHDAQCENTPEKE	Phosphorylation	T426	-0,35	38,67
	QDIDLGVSREVFDFSQRR	Phosphorylation	S33	2,17	72,76
	GENDKSLHLLKK	Phosphorylation	S549	-2,39	21,73
	EKGENDKSLHLLKK	Phosphorylation	S549	2,95	29,2
	SLHLLKK	Phosphorylation	S549	0,99	76,67
	SKKPDVKK	Phosphorylation	S597	-1,18	13,43
	TPVHSSGDMVQPLSPSQGQSTHVHDAQCENTPEKELPVSPGHRK	Phosphorylation	T395	-3,7	40,86
	TPFTKDK	Phosphorylation	T439	-0,76	49,55
NRF2	TPVHSSGDMVQPLSPSQGQSTHVHDAQCENTPEKE	Phosphorylation	T425	1,24	38,71
	SLHLLK	Phosphorylation	S549	1,38	22,88
	TPFTKDK	Phosphorylation	T439	0,24	49,85

B

Phosphorylation site	MS area NRF2	MS area MAPK15+NRF2
T395	-	7,97E+04
T425	2,71E+05	3,70E+06
T439	9,15E+02	1,06E+06

Fig. 13 (**A**) List of the NRF2 sites of phosphorylations found with mass spectrometry analysis performed after kinase assay. "Delta (ppm)" indicates the mass difference between the theoretical mass of the peptide and the experimental measured mass computed by using the following formula: Delta (ppm) = 1.000.000 x ([Mono Mass Exp. – Mono Mass Theo.] x Mono Mass Theo.). "RT" shows the retention time range with the most abundant MS area. Proline-directed threonine phosphorylation sites are indicated in red. (**B**) List of the proline-directed threonine phosphorylation sites of NRF2 protein.

Two of the three residues, specifically Thr395 and Thr439, were already identified to represent site of phosphorylation for cyclin-dependent kinase-5 (CDK5). Indeed, Jimenez-Blasco *et al*. (2015) demonstrated that p35-CDK5 complex phosphorylates NRF2 in Thr395, Ser433 and Thr439 promoting NRF2 nuclear translocation and inducing expression of antioxidant genes in astrocytes (Jimenez-Blasco *et al*., 2015) Starting from this assumption, we hypothesize that MAPK15 could have the same role of CDK5 in promoting NRF2 nuclear translocation. To assess it, we made up a protein cytoplasm/nucleus fractionation of 293T cells treated with H_2O_2 and FCCP, and we observed that NRF2 nuclear translocation is strongly induced in control (siSCR) treated sample, however it is intensely impaired when MAPK15 is depleted (**Fig. 14A-B**).

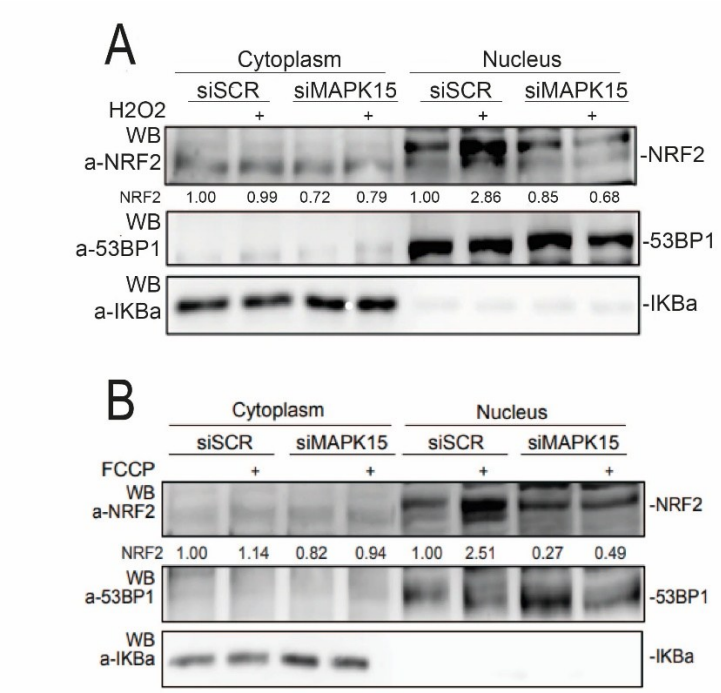

Fig. 14 (**A**) One representative WB experiments of three of lysates of 293T cells downregulated for MAPK15 (siMAPK15) compared to control (siSCR) treated with H_2O_2 (300 µM for 1 h) and subjected to nuclear/cytosolic fractionation. (**B**) Same as (**A**) but treated with FCCP (15 µM for 1 h).

Knowing that a dysregulated NRF2-dependent antioxidant response leads to intracellular ROS increment (Kovac *et al*., 2015; Yeang *et al*., 2012), to further confirm the activation of NRF2 by MAPK15, we transfected 293T cell line with empty vector or MAPK15 wild type (WT) or MAPK15 mutant impaired for its kinase domain (kinase dead: KD) and observed the intracellular ROS amount using CM-H2DCFDA florescent probe. The overexpression of MAPK15 WT, leads to a reduction of intracellular ROS in comparison to empty vector, whereas MAPK15 KD fails causing ROS increase, albeit slightly (**Fig. 15**).

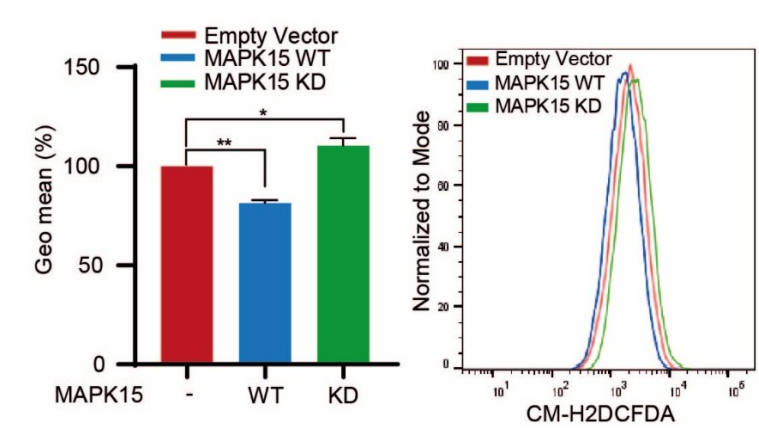

Fig. 15 Histogram of Geometric Mean Fluorescent Intensity (GeoMFI) bars of CM-H2DCFDA fluorescence analyzed by Fluorescence-Activated Cell Sorting (FACS) of 293T cells transfected with MAPK15 WT or MAPK15 KD plasmid. Bars represent the average ± S.D. of 3 independent experiments.

Accordingly with the increment of intracellular ROS, the antioxidant response is impaired when cells express MAPK15 KD mutant protein, as demonstrated by real-time quantitative PCR of NRF2 target genes (NQO1 and HO-1) (**Fig. 16A**) and so does the NRF2 transcriptional activity, as demonstrated by luciferase assay (**Fig. 16B**). We validated the data even at protein level, demonstrating that when MAPK15 lacks its functioning kinase domain it is unable to induce NRF2 at the same level as the WT counterpart in transfected 293T cells in untreated and after oxidative stimulus (**Fig. 16C**).

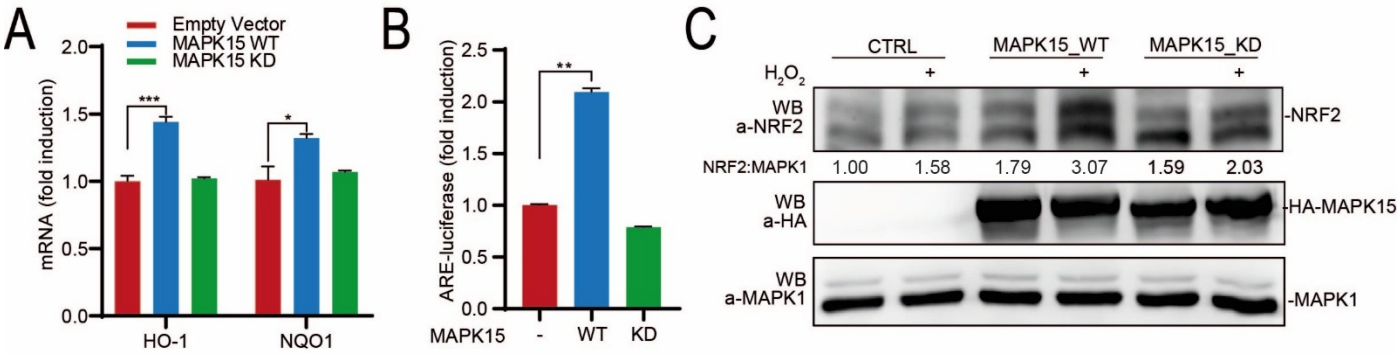

Fig. 16 *(***A**) Relative mRNA levels of indicated genes of 293T cells transfected with MAPK15 WT or MAPK15 KD plasmid. All real-time quantitative PCR results represent the average ± S.D. of three independent experiments. (**B**) Luciferase assay of 293T cells co-transfected with ARE luciferase reporter vector plus empty vector or MAPK15 WT or MAPK15 KD plasmid. All luciferase results represent the average ± S.D. of three independent experiments. (**C**) One representative WB experiment of three of lysates of 293T cells transfected with empty vector or MAPK15 WT or MAPK15 KD plasmid treated with H_2O_2 (300 µM for 1 h).

At last, to produce the inhibition of MAPK15 with a pharmacological approach, we treated cells with Ro-318220 (Colecchia *et al*., 2012), TMCB (Pagano *et al*., 2008) or sorafenib (https://www.kinase-screen.mrc.ac.uk/inhibitor-and-results/16). In this manner we assessed the behavior of endogenous MAPK15 inhibition and confirmed the significant reduction of NRF2 protein level both in basal condition and upon cellular exposure to oxidative stress by H_2O_2 stimulation (**Fig. 17A-B-C**).
Overall, the experiments support the hypothesis that MAPK15 directly phosphorylates NRF2 supporting its nuclear translocation and transcription of NRF2 downstream genes.

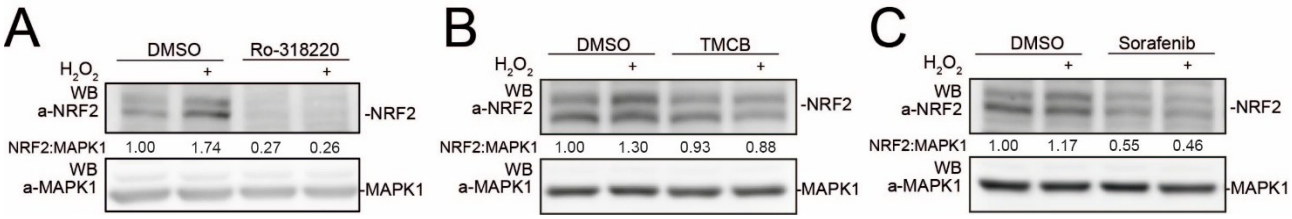

Fig. 17 (**A**) One representative WB experiment of three of lysates of 293T cells treated sequentially with vehicle or Ro-318220 (2 μM for 6 h) and with vehicle or H_2O_2 during the last hour of treatment (300 μM for 1 h). (**B**) Same as in (**A**), but cells were treated with vehicle or TMCB (10 μM for 24 h). (**C**) Same as in (**A**), but cells were treated with vehicle or Sorafenib (10 μM for 24h).

4.4. MAPK15 stabilizes NRF2 protein

Under normal conditions, NRF2 has a half-life of about 10-30 minutes, and its turnover is mediated by KEAP1. KEAP1 acts as adaptor proteins for cullin 3 (CUL3)-based E3 ubiquitin ligases sending NRF2 to proteasome degradation. As a result of the oxidative stress, KEAP1 is oxidated and inactivated leading to NRF2 stabilization, incrementing its half-life, and nuclear translocation (Baird & Yamamoto, 2020; Tonelli *et al*., 2018). As NRF2 protein levels were clearly affected by modulating MAPK15 expression (**Fig. 6-7-8-9-10**) we decided to deeply investigate the NRF2 modulation during time. In order to do this, we co-transfected 293T cells with NRF-MYC-FLAG plasmid and empty vector or MAPK15 WT and treated cells with cycloheximide to inhibit protein synthesis. The WB experiment clearly reveals that NRF2 protein is mostly accumulated through time when MAPK15 is overexpressed, compared to control (**Fig. 18**).

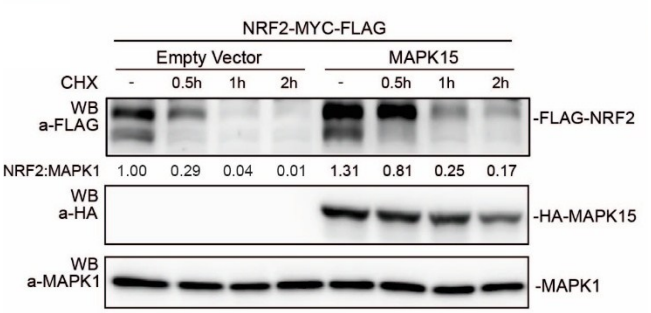

Fig. 18 One representative WB experiment of three of lysates of 293T cells co-transfected with NRF2-MYC-FALG and empty vector or MAPK15 plasmid treated with CHX (50 μM for different times).

4.5. MAPK15 induces PKC-dependent phosphorylation of NRF2 on Ser40 residue

According to the literature, after oxidative stimulus, NRF2 is phosphorylated on Ser40 residue by protein kinase-C (PKC) and this phosphorylation allows NRF2 to escape from proteasomal degradation. Taking advantage from anti-phospho-NRF2-Ser40, we co-transfected with NRF2 and with empty vector or MAPK15 WT or MAPK15 KD plasmids in 293T cells, and we found that MAPK15 WT is able to increase NRF2 Ser40 phosphorylation, both basal condition and under oxidative stimulation (H_2O_2) and that MAPK15 KD is unable to induce phosphorylation (**Fig. 19A**). To confirm this data, NRF2 S40A mutant, where serine was replaced with alanine, was co-transfected in 293T cells together with MAPK15 WT or empty vector and compared with corresponding NRF2 WT control. MAPK15 WT successfully increases NRF2 WT protein level but fails to increase NRF2

S40A mutant (**Fig. 19B**). Correspondently, MAPK15 downregulation through siRNA (Fig. 20A-B) inhibits Ser40 phosphorylation normally induced by oxidative stress (**Fig. 19C**). The role of MAPK15 in Ser40 phosphorylation was also confirmed by immunofluorescence assay analyzed by confocal microscopy (**Fig. 21**).

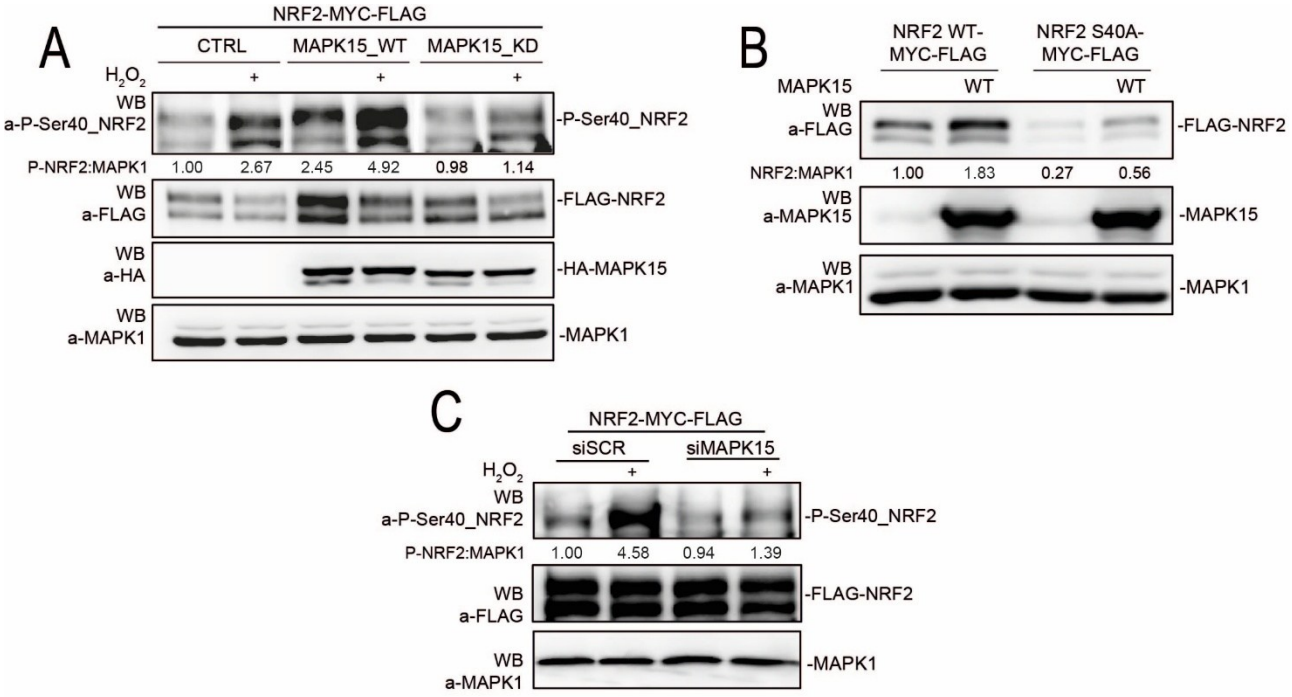

Fig. 19 (**A**) One representative WB experiment of three of lysates of 293T cells co-transfected withNRF2-MYC-FLAG and empty vector or MAPK15 WT or MAPK15 KD plasmid treated with H_2O_2 (300 µM for 1 h). (**B**) One representative WB experiment of three of lysates of 293T cells co-transfected with MAPK15 and NRF2 WT-MYC-FLAG or NRF2-MYC-FLAG S40A. (**C**) One representative WB experiment of three of lysates of 293T cells downregulated for MAPK15 (siMAPK15) compared to control (siSCR) and transfected with NRF2-MYC-FLAG plasmid, treated with H_2O_2 (300 µM for 1 h).

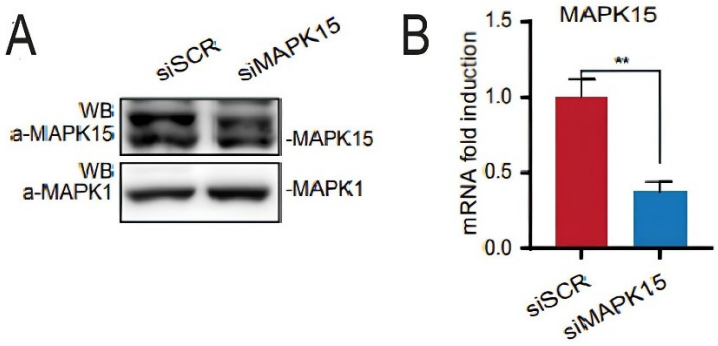

Fig. 20 (**A**) One representative WB experiment of three of lysates of 293T cells downregulated for MAPK15 (siMAPK15) compared to control (siSCR). (**B**) Relative mRNA levels of MAPK15 in HeLa cells downregulated for MAPK15 (siMAPK15) compared to control (siSCR). All real-time quantitative PCR results represent the average ± S.D. of three independent experiments.

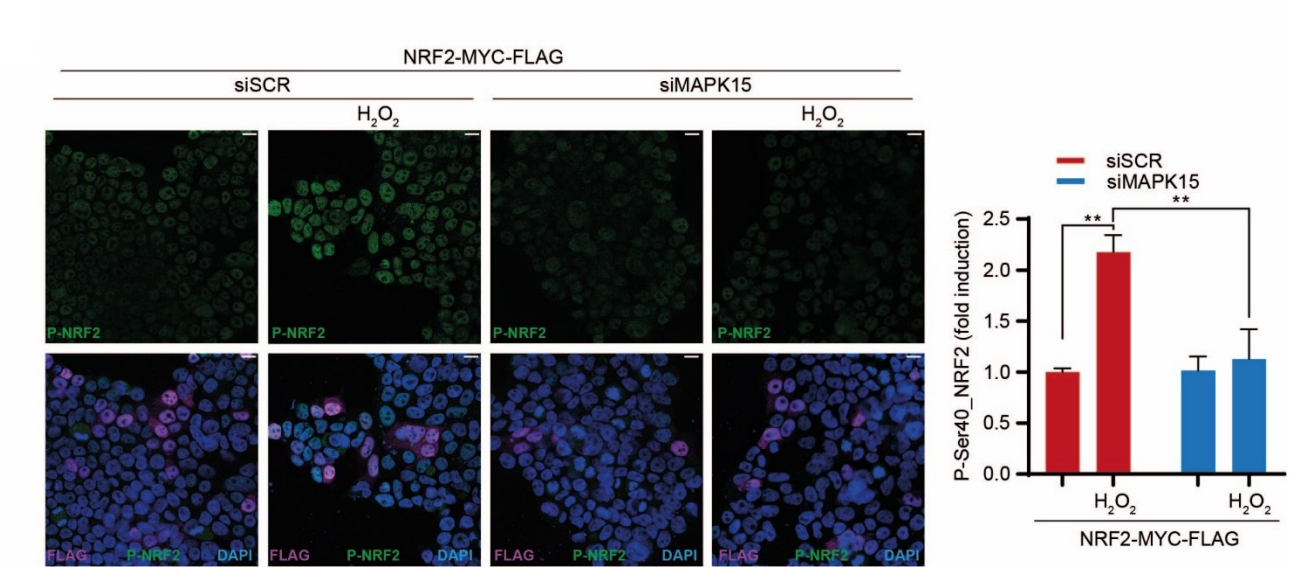

Fig. 21 Representative images of immunofluorescence assay of 293T cells downregulated for MAPK15 (siMAPK15) compared to control (siSCR) treated with H_2O_2 (300 µM for 1 h). The histogram represents the quantification of fluorescent intensity of indicated protein from five representative microscopy fields signal per cell of three different experiments ± SD. Scale bars correspond to 10 µm.

As the NRF2 Ser40 is not followed by proline, it does not represent the typical phosphorylation residue target for MAPK15. Therefore, we hypothesize that MAPK15 may induce phosphorylation through PKC. Indeed, we confronted the capability of MAPK15 to phosphorylate, and in turn activate PKC with two positive controls: a general oxidative stimulus (H_2O_2) and TPA, a chemical inducer of PKC. Through WB assay on 293T cells, we observed that MAPK15 is actually able to induce PKC phosphorylation at the same level of positive controls (**Fig. 22**).

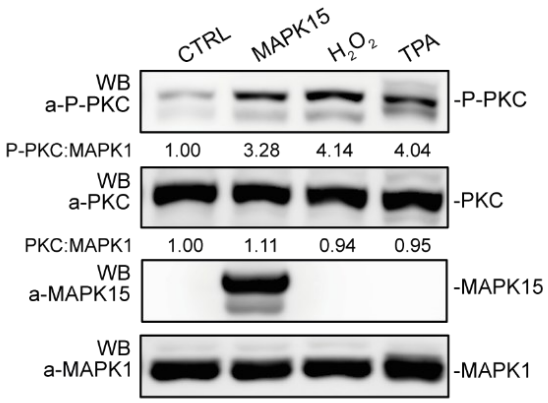

Fig. 22 One representative WB experiment of three of lysates of 293T cells transfected with MAPK15 or empty vector plasmid or treated with H_2O_2 (300 µM for 1 h) or TPA (200 nM for 1 h).

To strengthen our results, we used GO6983, an inhibitor of PKC activity, to confirm whether MAPK15 acts or not on NRF2 through PKC. We showed that GO6983 treatment strongly reduced MAPK15-dependent NRF2 Ser40 phosphorylation (**Fig. 23A**), as well as NRF2 transcriptional activity demonstrating the existence of MAPK15-PKC-NRF2 axis (**Fig. 23B**).

Taken together, the data suggests that MAPK15 supports NRF2 antioxidant response by stabilizing the protein through indirect phosphorylation at Ser40 mediated by PKC, which in turn may be directly or indirectly phosphorylated by MAPK15.

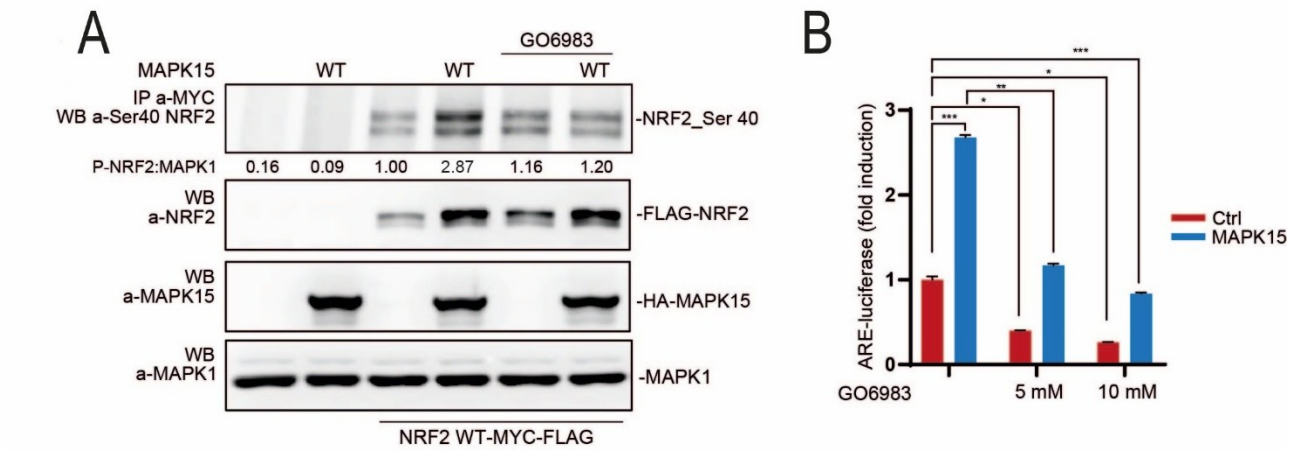

Fig. 23 (**A**) One representative WB experiment of three of lysates of 293T cells co-transfected with NRF2 WT-MYC-FLAG and HA-MAPK15 WT or empty vector plasmid, treated with GO6983 (10 μM for 2 h) and immunoprecipitated with anti-MYC antibody. Total lysates were even analyzed. (**B**) Luciferase assay of 293T cells transfected with ARE luciferase reporter vector plasmid and treated with GO6983 (10 μM for 2 h). All luciferase results represent the average ± S.D. of three independent experiments.

4.6. NRF2 impaired activity after MAPK15 downregulation is responsible for intracellular ROS increment and DNA damage

We have already shown the increase of intracellular ROS when MAPK15 kinase activity is abolished (**Fig. 15**) and in past works it was demonstrated that the MAPK15 downregulation induces increment of mitochondrial ROS and consequent DNA damage due to impairment of mitophagy (Franci *et al*., 2022) and that MAPK15 upregulation prevents DNA damage promoting autophagy (Rossi *et al*., 2016) an already known mechanism to be important to maintain genome stability (Bonora *et al*., 2016; Vessoni *et al*., 2013).

As NRF2 is the master regulator of the antioxidant response and we have demonstrated that MAPK15 modulates its activity, it is reasonable to assume that the impairment of NRF2 function upon MAPK15 depletion or inactivation contributes, at least in part, to the increase in ROS levels and DNA damage. To demonstrate this hypothesis, we overexpressed NRF2 in HeLa cell line silenced for MAPK15, rescuing the MAPK15-depleted phenotype (**Fig. 24A**). As consequence, the intracellular ROS level significantly decreases, returning almost at baseline level when NRF2 is overexpressed in siMAPK15 cells (**Fig. 24B**).

Regarding DNA damage, we observed an increase γH2A.X fluorescence when MAPK15 is downregulated. However, NRF2 rescue siMAPK15 cells strongly decreased DNA damage compared to the not rescued condition (**Fig. 24C**).

Taken together these data improve our understanding of the mechanisms of intracellular ROS and DNA damage growth when MAPK15 is absent. Specifically, they indicate that the increase in oxidative stress and consequent DNA damage is not only linked to impaired mitophagy and autophagy, as reported by Franci *et al*. (2022) and Rossi *et al*. (2016), but also to the disruption of the NRF2 defense pathway.

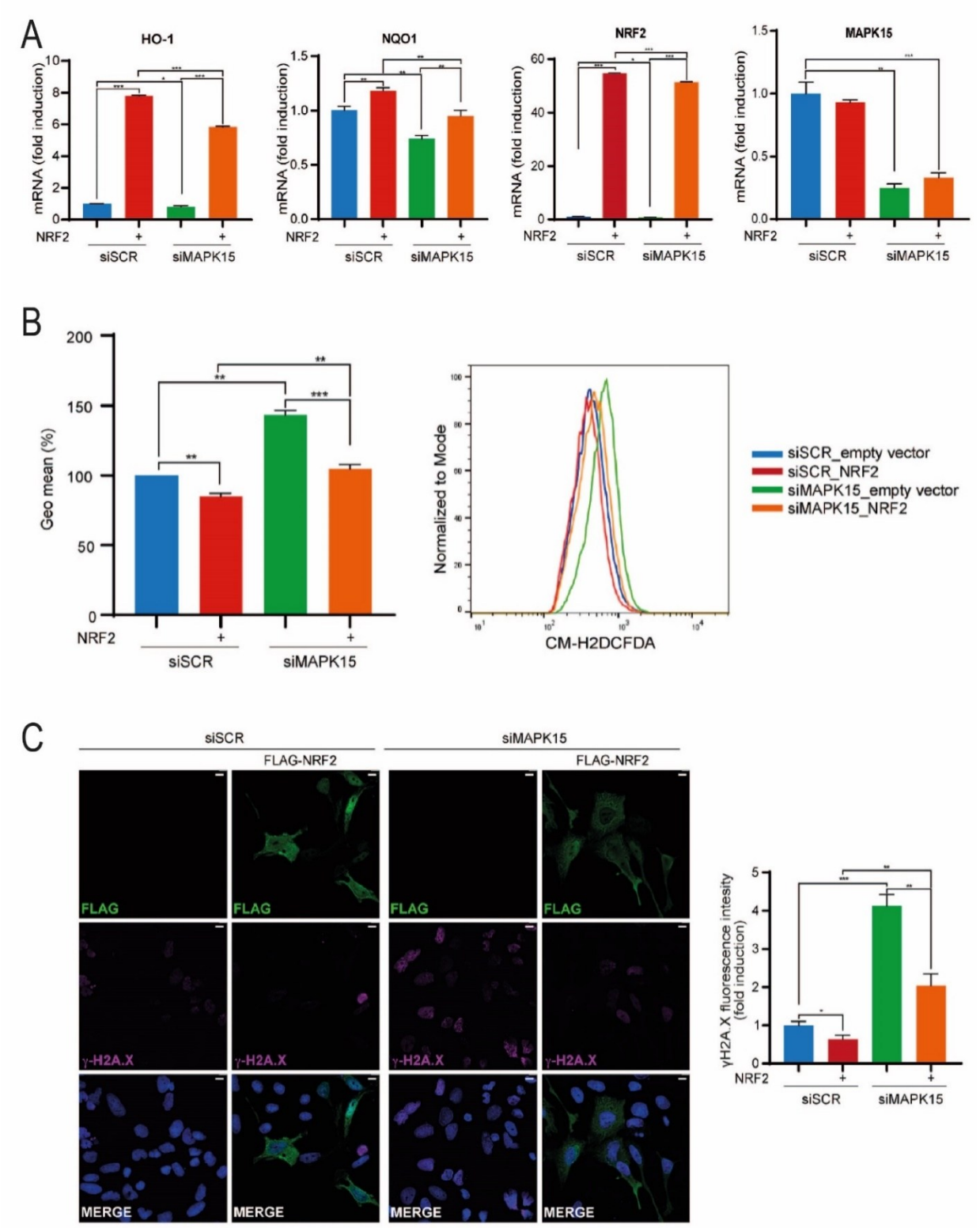

Fig. 24 (**A**) Relative mRNA levels of HeLa cells downregulated for MAPK15 (siMAPK15) compared to control (siSCR) and transfected with empty vector or NRF2 plasmid. All real-time quantitative PCR results represent the average ± S.D. of three independent experiments. (**B**) Histogram of Geometric Mean Fluorescent Intensity (GeoMFI) bars of CM-H2DCFDA fluorescence analyzed by Fluorescence-Activated Cell Sorting (FACS) of HeLa cells downregulated for MAPK15 (siMAPK15) compared to control (siSCR) and transfected with empty vectori or NRF plasmid. Bars represent the average ± S.D. of 3 independent experiments. (**C**) Representative images of immunofluorescence assay of HeLa cells downregulated for MAPK15 (siMAPK15) compared to control (siSCR) and transfected with empty vector or NRF2-

MYC-FLAG. The histogram represents the quantification of fluorescent intensity of indicated protein from five representative microscopy fields signal per cell ± SD. Scale bars correspond to 10 μm.

4.7. MAPK15 enhanced the NRF2-mediated antioxidant response in human lung cell lines

It is well established that cigarette smoke is a major risk factor for cancer, as well as for respiratory and cardiovascular diseases, and that the oxidative stress it induces contributes to the onset of smoke-related pathologies (Seo *et al.*, 2023). Environmental stimuli such as smoke have a particularly strong impact on organs directly exposed to the external environment, notably the lungs. In addition, MAPK15 is highly expressed in pulmonary tissues (Abe *et al.*, 2002).
In order to assess the role of MAPK15 in lungs, we treated hAEC cell line, normal human epithelial lung cells used as model to study pulmonary response, downregulated for MAPK15 (**Fig. 25A-B**) with condensed smoke extract (CSE).

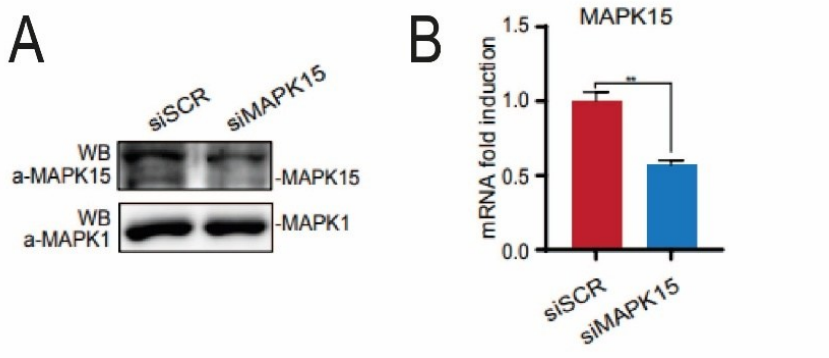

Fig. 25 (**A**) One representative WB experiment of three of lysates of HeLa cells downregulated for MAPK15 (siMAPK15) compared to control (siSCR). (**B**) Relative mRNA levels of MAPK15 in HeLa cells downregulated for MAPK15 (siMAPK15) compared to control (siSCR). All real-time quantitative PCR results represent the average ± S.D. of three independent experiments.

The extract significatively increases the intracellular ROS both in siSCR and siMAPK15 samples but to a greater extent with siMAPK15 samples (**Fig. 26A**). To deal with ROS increment, the cells respond increasing NRF2 protein level activating antioxidant response but in a less efficient manner (about 50% less) when MAPK15 is downregulated (**Fig. 26B**).
Moreover, pharmacological inhibition of MAPK15 using Ro-318220, TMCB, and Sorafenib, significatively reduced NRF2 protein levels both in unstimulated conditions and upon CSE treatment in hAEC (**Fig. 26C-D-E**) and in 293T cells (**Fig. 27A-B-C**), supporting the possibility of developing new drugs modulating cellular responses to oxidative stress by acting on MAPK15

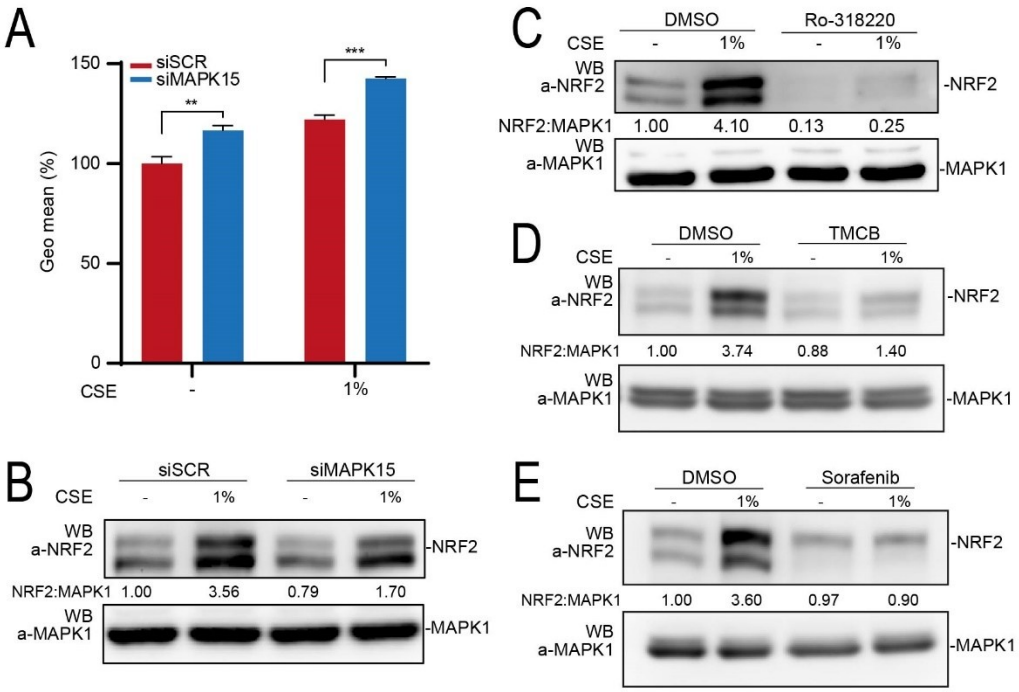

Fig. 26 (**A**) Histogram of Geometric Mean Fluorescent Intensity (GeoMFI) bars of CM-H2DCFDA fluorescence analyzed by Fluorescence-Activated Cell Sorting (FACS) of hAEC cells downregulated for MAPK15 (siMAPK15) compared to control (siSCR) and treated with CSE (1% for 4 h). Bars represent the results represent the average ± S. D of 3 independent experiments. (**B**) One representative WB experiment of three of lysates of hAEC cells downregulated for MAPK15 (siMAPK15) compared to control (siSCR) and treated with CSE (1% for 4 h). (**C**) One representative WB experiment of three of lysates of hAEC cells treated with Ro-318220 (2 μM for 6h) or vehicle and during the last hours of treatment with CSE (1% for 4 h). (**D**) One representative WB experiment of three of lysates of hAEC cells treated with TMCB (10 μM, for 24 h) or vehicle and during the last hours of treatment with CSE (1% for 4 h). (**E**) One representative WB experiment of three of lysates of hAEC cells treated with Sorafenib (10 μM, for 24 h)or vehicle and during the last hours of treatment with CSE (1% for 4 h).

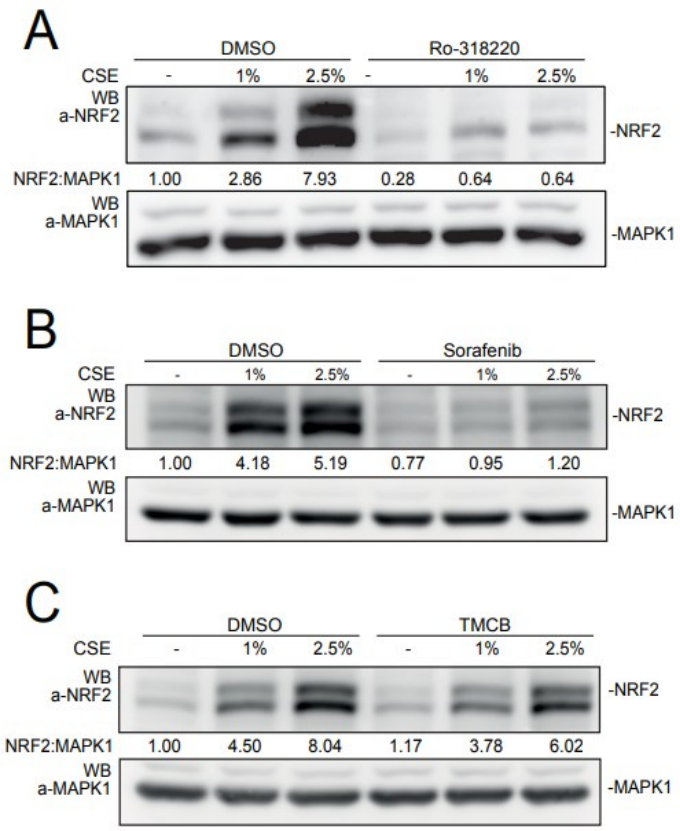

Fig. 27 (**A**) One representative WB experiment of three of lysates of 293T cells treated with Ro-318220 (2 μM for 6h) or vehicle and during the last hours of treatment with CSE (1% or 2.5% for 4 h). (**B**) One representative WB experiment of three of lysates of 293T cells treated with Sorafenib (10 μM for 10 h) or vehicle and during the last hours of treatment with CSE (1% or 2.5% for 4 h). (**C**) One representative WB experiment of three of lysates of 293T cells treated with TMCB (10 μM for 24 h) or vehicle and during the last hours of treatment with CSE (1% or 2.5% for 4 h).

CSE, moreover, strongly induces NRF2 nuclear translocation, as demonstrated by nuclear-cytoplasmic fractionation resolved by WB, while MAPK15 downregulation prevented its translocation (**Fig. 28A**), reinforcing the role of MAPK15 in supporting NRF2 nuclear translocation. In the nucleus, NRF2 binds to the antioxidant response element in DNA and induces the transcription of several downstream antioxidant genes, such as *HO-1*, *NQO1*, *MGST1*, *GCLM*, *GCLC*, and *AKR1B10*. In this context, gene induction was markedly reduced when MAPK15 was silenced, as assessed by real-time quantitative PCR (**Fig. 28B**).

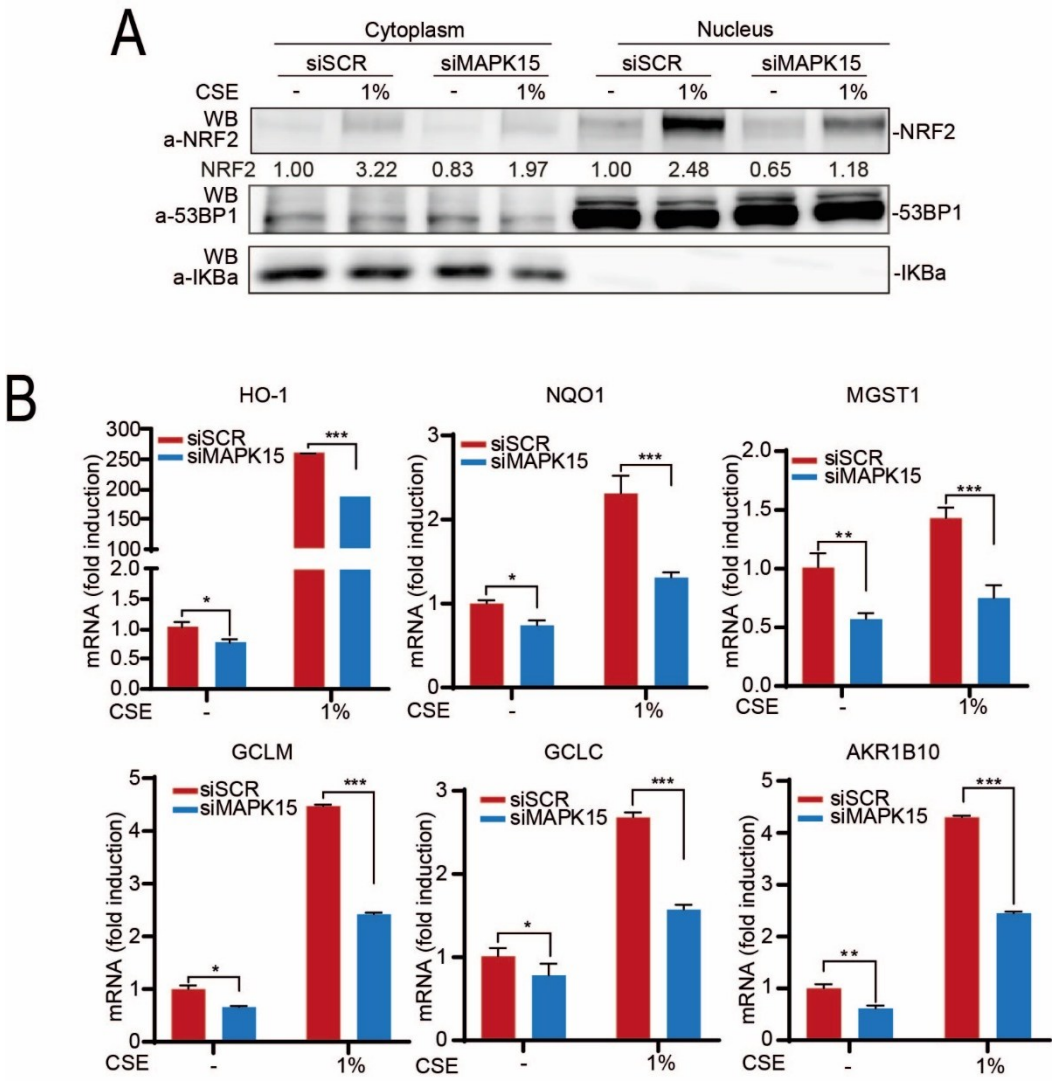

Fig. 28 (**A**) One representative WB experiments of three of lysates of hAEC cells downregulated for MAPK15 (siMAPK15) compared to control (siSCR) treated with CSE (1% for 4 h) and subjected to nuclear/cytosolic fractionation. (**B**) Relative mRNA levels of indicated genes of hAEC cells downregulated for MAPK15 (siMAPK15) compared to control (siSCR) and treated with CSE (1% for 4 h). All real-time quantitative PCR results represent the average ± S.D. of three independent experiments.

Interestingly, among these genes, AKR1B10 stood out as the only one expressed at detectable levels exclusively in hAEC cells among all cell types analyzed in our study (**Fig. 29A**). Its expression was significantly reduced at both the mRNA (**Fig. 28B**) and protein levels (**Fig. 29B**) following MAPK15 downregulation, in both basal conditions and upon CSE stimulation.

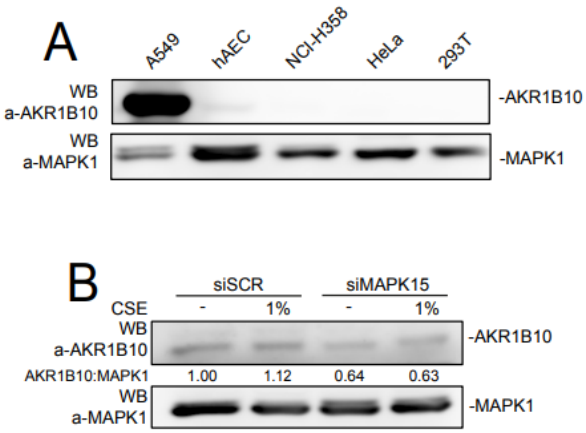

Fig. 29 (**A**) One representative WB experiment of three of lysates of A549, hAEC, NCI-H358, HeLa and 293T cells. (**B**) One representative WB experiment of three of lysates of hAEC cells downregulated for MAPK15 (siMAPK15) compared to control (siSCR) and treated with CSE (1% for 4 h).

Next, we evaluated whether MAPK15-dependent NRF2 regulation occurs even in lung cancer cell line, specifically in NCI-H358 cells, isolated from non-small cell lung cancer. Accordingly with all the other cell lines used in our research, downregulation of MAPK15 in NCI–H358 cells (**Fig. 30A-B**), and the simultaneously CSE treatment increase ROS levels (**Fig. 31A**) and reduce NRF2 protein levels (**Fig. 31B**). The same effect can also be achieved using three different MAPK15 pharmacological inhibitors, Ro-318220 (**Fig. 31C**), TMCB (**Fig. 31D**) and Sorafenib (**Fig. 31E**).

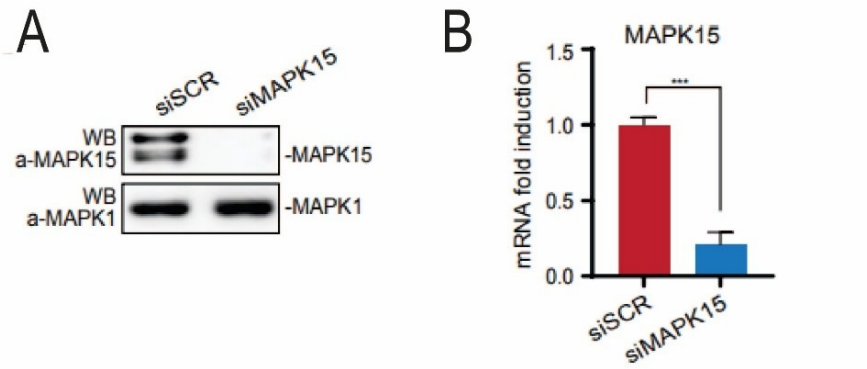

Fig. 30 (**A**) One representative WB experiment of three of lysates of HeLa cells downregulated for MAPK15 (siMAPK15) compared to control (siSCR). (**B**) Relative mRNA levels of MAPK15 in HeLa cells downregulated for MAPK15 (siMAPK15) compared to control (siSCR). All real-time quantitative PCR results represent the average ± S.D. of three independent experiments.

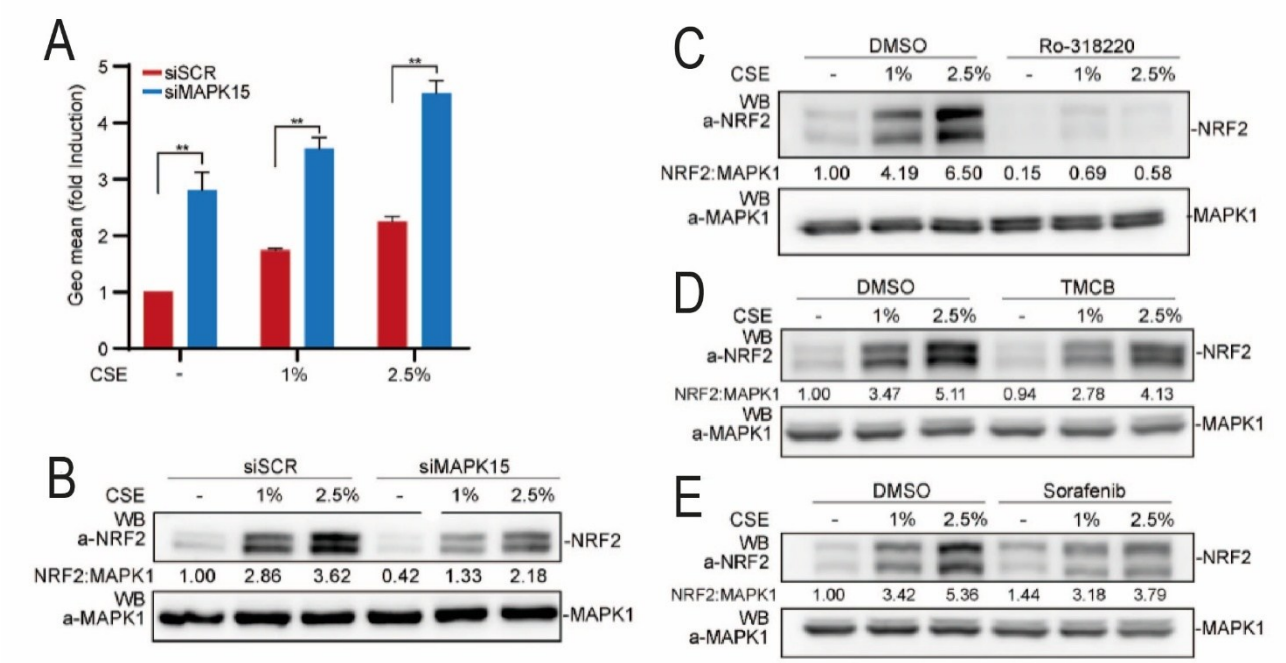

Fig. 31 (**A**) Histogram of Geometric Mean Fluorescent Intensity (GeoMFI) bars of CM-H2DCFDA fluorescence analyzed by Fluorescence-Activated Cell Sorting (FACS) of NCI-H358 cells downregulated for MAPK15 (siMAPK15) compared to control (siSCR) and treated with CSE (1% or 2.5% for 4 h). Bars represent the average ± S.D. of 3 independent experiments. (**B**) One representative WB experiment of three of lysates of NCI-H358 cells downregulated for MAPK15 (siMAPK15) compared to control (siSCR) and treated with CSE (1% or 2.5% for 4 h). (**C**) One representative WB experiment of three of lysates of hAEC cells treated with Ro-318220 (2 μM for 6 h) or vehicle and during the last hours of treatment with CSE (1% or 2.5% for 4 h). (**D**) One representative WB experiment of three of lysates of NCI-H358 cells treated with TMCB (10 μM for 24 h) or vehicle and during the last hours of treatment with CSE (1% or 2.5% for 4 h). (**E**) One representative WB experiment of three of lysates of NCI-H358 cells treated with Sorafenib (10 μM for 24 h) or vehicle and during the last hours of treatment with CSE (1% or 2.5% for 4 h).

Importantly, we confirmed the inhibitory effect of MAPK15 downregulation on NRF2 nuclear translocation, particularly evident after CSE treatment (**Fig. 32**).

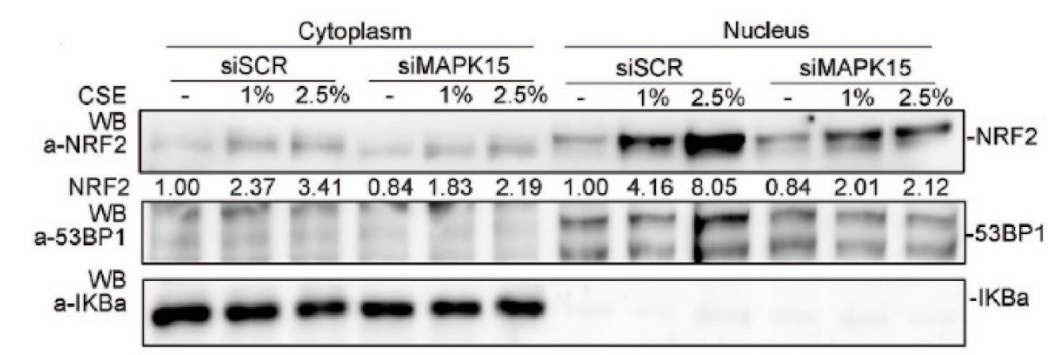

Fig. 32 One representative WB experiments of three of lysates of NCI-H358 cells downregulated for MAPK15 (siMAPK15) compared to control (siSCR) treated with CSE (1% or 2.5% for 4 h) and subjected to nuclear/cytosolic fractionation.

Consequently, the transactivation of NRF2 is impaired when MAPK15 is downregulated, as demonstrated by ARE-luciferase assay (**Fig. 33A**), while overexpression of MAPK15 leads to an increase in transcriptional activity to higher level compared to empty vector control especially after CSE treatment (**Fig. 33B**). Accordingly, MAPK15 downregulation reduces the expression of several

NRF2 target genes, in unstimulated NCI–H358 cells, while prevents their increase triggered by oxidative stress induced by CSE (**Fig. 33C**).

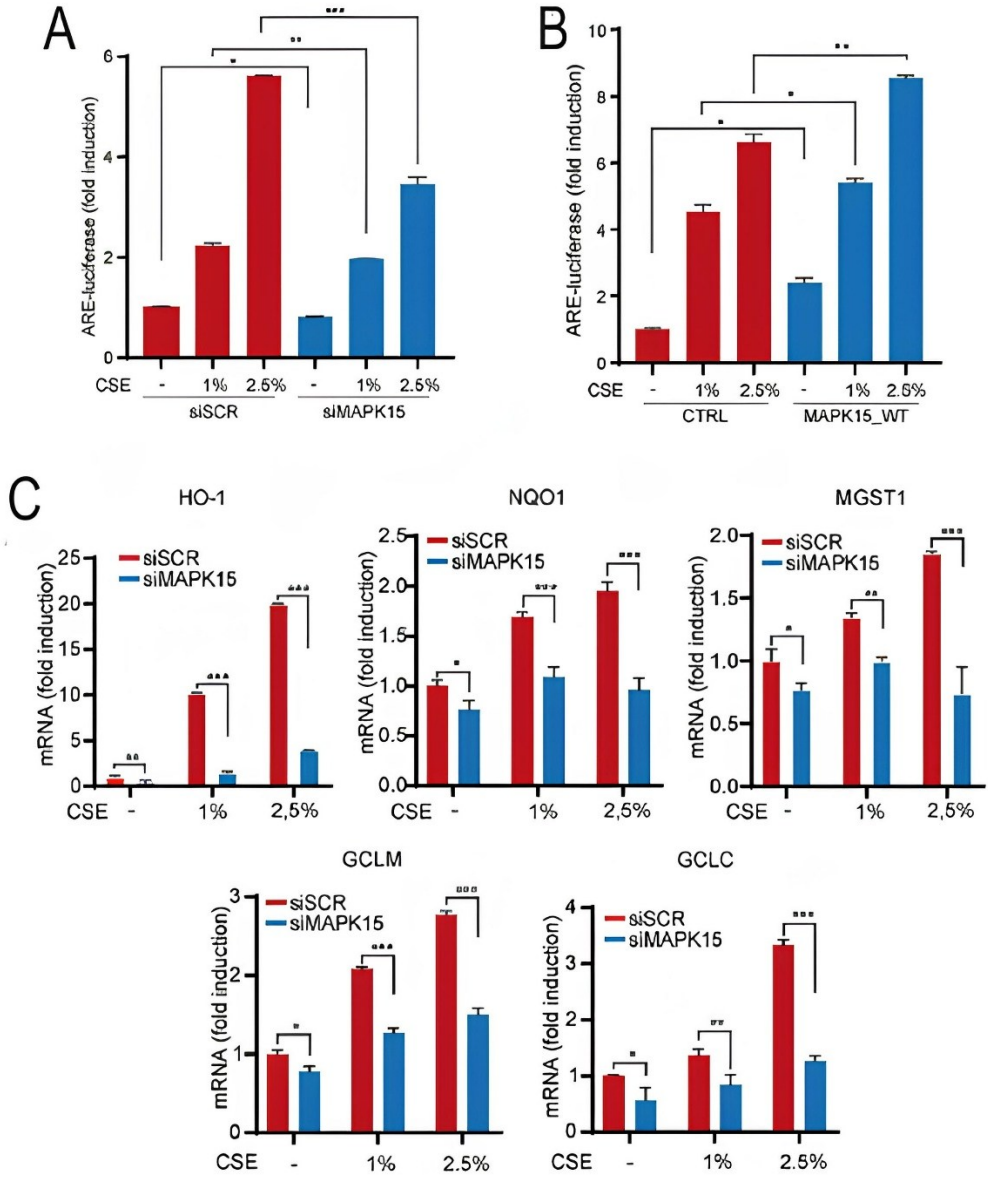

Fig. 33 (**A**) Luciferase assay of NCI-H358 cells downregulated for MAPK15 (siMAPK15) compared to control (siSCR) and transfected with ARE luciferase reporter vector plasmid and treated with CSE (1% or 2.5% for 4 h). All luciferase results represent the average ± S.D. of three independent experiments. (**B**) Luciferase assay of NCI-H358 cells co-trasfected with MAPK15 or control plasmid and ARE luciferase reporter vector plasmid and treated with CSE (1% or 2.5% for 4 h). All luciferase results represent the average ± S.D. of three independent experiments. (**C**) Relative mRNA levels of indicated genes of NCI-H358 cells downregulated for MAPK15 (siMAPK15) compared to control (siSCR) and treated with CSE (1% or 2.5% for 4 h). All real-time quantitative PCR results represent the average ± S.D. of three independent experiments.

The experiments performed on human lung cell lines, both normal and cancerous, demonstrate the role of MAPK15 in enhancing the NRF2-mediated antioxidant response, particularly important in such organs continuously in contact, not only with oxygen, but also with all types of environmental pollutants, as smoke.

4.8. Endogenous MAPK15 regulates NRF2 protein level in non-small cell lung cancer carrying Loss Of Function mutation in KEAP1 gene

We also studied the protein expression of NRF2 and its target gene, HO-1, in A549 and NCI-H460 cell lines, conventionally used as models for non-small cell lung cancer (NSCLC). We didn't perform experiments with oxidative stimulation since both carry a mutation loss of function (LOF) on KEAP1 gene that lead to constitute activation of NRF2**.** LOF Mutation on KEAP1 or gain of function are common in NSCLC and confer resistance to chemotherapy, radiotherapy, and targeted agents (Scalera *et al*., 2022). After MAPK15 downregulation (**Fig. 34**) NRF2 and HO-1 proteins decrease significantly in both A549 and NCI-H460. We can say that also in these two cell lines, MAPK15 controls NRF2 protein level and presumably its activity as even one of its target gene (HO-1) is downregulated at protein level (**Fig. 35**).

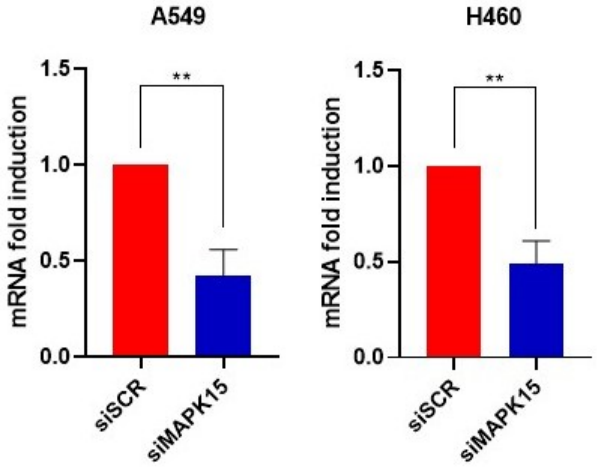

Fig. 34 Relative mRNA levels of MAPK15 in A549 and NCI-H460 cells downregulated for MAPK15 (siMAPK15) compared to control (siSCR). All real-time quantitative PCR results represent the average ± S.D. of three independent experiments.

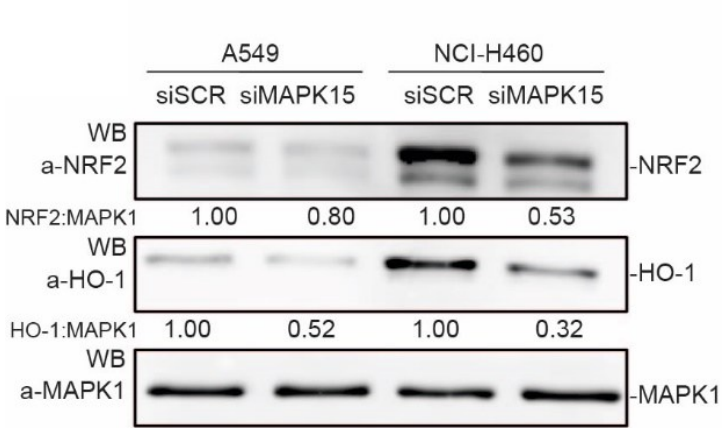

Fig. 35 One representative WB experiments of three of lysates of A549 and NCI-H460 cells downregulated for MAPK15 (siMAPK15) compared to control (siSCR).

Therefore, endogenous MAPK15 regulates NRF2 protein level and, in turn, HO-1 level even in NSCLC cell lines, suggesting that its role could be interesting in the treatment also for lung cancers where NRF2 pathway is hyperactivated.

5. Discussion

MAPK15 is the last discovered member of the mitogen-activated protein kinase family, and its biological function is still not fully understood. The study presented here sheds new light on the role of MAPK15 in contributing to regulation of NRF2-dependent antioxidant responses. The results obtained with different cell lines, isolated from various types of tissues and tumors, strongly suggest that this function of MAPK15 is a general mechanism shared by cells and not relegated to a specific phenotype or genotype context.

In previous studies, the MAPK15 depleted phenotype was described in some aspects and the kinase was linked to fundamental cellular processes involved in maintaining redox balance and genome stability. Importantly, these two elements are intrinsically related as, during DNA replication or transcription, reactive oxygen species (ROS) can chemically induce missense mutations, truncation mutations, or even cause DNA strand breaks (Li *et al*., 2025). Groehler & Lannigan (2010) also observed that, in cells exposed to ultraviolet-C (UVC), MAPK15 depletion led to an increase of DNA damage compared to cells with normal MAPK15 expression, and that the rescue of MAPK15 expression resulted in a mitigation of DNA damage thanks to the ability of MAPK15 to stabilize the binding between chromatin and PCNA, a protein involved in DNA repair. Although authors didn't investigate the level on intracellular ROS, it is well established that UV induces generation of ROS (de Jager *et al*., 2017) and, in the light of the results achieved, we can speculate that a rescue of MAPK15 could contribute to the reduction of DNA damage, even for its function to support NRF2 dependent antioxidant response. MAPK15 was also demonstrated to control the rate of basal cellular autophagy during starvation and in absence of stimuli (Colecchia *et al*., 2012). It is well recognized that autophagy helps to eliminate irreversibly oxidized biomolecules from cells and, for this reason, it can be considered an integral part of antioxidant defenses and DNA repair mechanisms (Filomeni *et al*., 2015). Furthermore, Franci *et al*. (2022) found out that MAPK15 regulates mitophagy by promoting ULK1 dependent phosphorylation of PRKN, thereby facilitating the recruitment of damaged mitochondria to autophagosomes and lysosomes (Franci *et al*., 2022). On the contrary, reduced MAPK15 expression impairs mitophagy process leading to an accumulation of damaged mitochondria and consequent increment of intracellular ROS and DNA damage. The molecular mechanism elucidated in the current study contributes to explain the MAPK15 depleted phenotype already analyzed in the previous studies, indicating the impairment of NRF2 dependent antioxidant response as one of the important causes of increment of intracellular ROS and DNA damage and clarifying that the presence of MAPK15 is one of the mechanisms supporting the genome stability and oxidative balance. The first evidence that MAPK15 could be involved in response to oxidative stress dates to 2006 when Klevernic *et al*. reported that hydrogen peroxide (H_2O_2) is able to stimulate the phosphorylation of MAPK15, activating the protein (Klevernic *et al*. 2006). The paper focused on the characterization of MAPK15 autophosphorylation and didn't investigate the cause of MAPK15 activation and its physiological role remained unknown. Now, in light of the findings reported in this study, we can explain that MAPK15 autoactivates after H_2O_2 treatment because of its role in the regulation of NRF2 dependent antioxidant response, and that it responds not only to H_2O_2, but also to carbonylcyanide-4-(trifluoromethoxy)-phenylhydrazone (FCCP) and condensed smoke extract (CSE) exposure, representing general sources of ROS. Moreover, we showed that the regulation of MAPK15 on NRF2 is not strictly correlated with presence of intracellular ROS, as the depletion of MAPK15 still impairs NRF2 pathway in cells treated with direct pharmacological NRF2 inducers

(sulforaphane and dimethyl fumarate). Therefore, given the MAPK15 role in reducing ROS and DNA damage, promoting autophagy and mitophagy and supporting PCNA activity, we can affirm that MAPK15 is involved in maintenance of genome stability.

Importantly, we bring evidence of direct interaction between MAPK15 and NRF2. Thanks to mass spectrometry analysis, we can say that MAPK15 directly phosphorylates three NRF2 residues, Thr395, Thr439 and Thr425. Two of them, Thr395 and Thr439, have been already reported to be targets of CDK5 and to promote NRF2 nuclear translocation (Jimenez-Blasco *et al*., 2015). In accordance, we observed that the absence of MAPK15 impairs the correct NRF2 nuclear translocation (**Fig. 36**). We also observed that MAPK15 promotes the activation of PKC that, in turn, phosphorylates Ser40 residue of NRF2 protein, contributing to protein stabilization as already described by Bloom and Jaiswal (2003) (**Fig. 36**). The mechanism by which MAPK15 activates PKC remains unknown and further studies are needed to address whether the phosphorylation is directly operated by MAPK15, or whether one or more proteins are required.

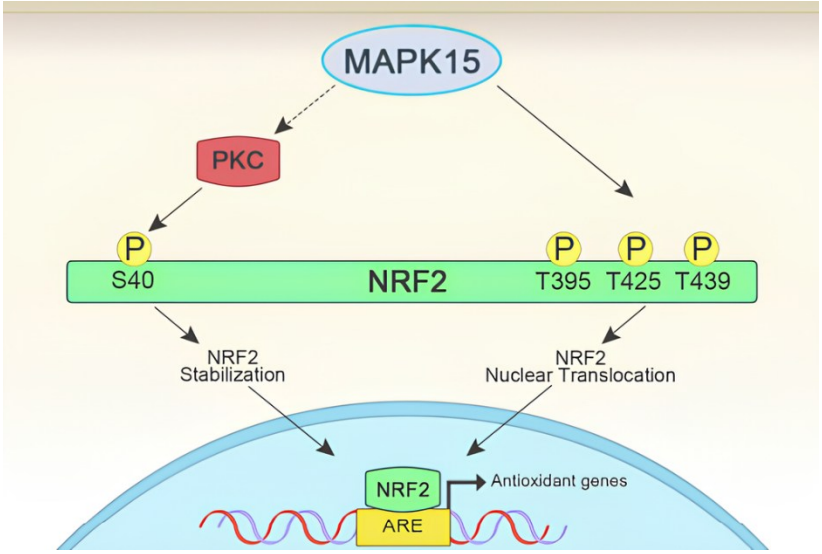

Fig. 36 Graphical model of MAPK15 mechanism of action on NRF2 regulation. MAPK15 directly phosphorylates NRF2 in three different threonine residues (395-425-439) promoting NRF2 nuclear translocation and activates PKC that, in turn, phosphorylates NRF2 serine 40 residue supporting protein stabilization.

NRF2 and ROS have dual and contrasting functions in the development of pathologies. Many diseases are correlated to oxidative stress, such as neurodegenerative diseases. A growing body of evidence suggests that oxidative damage and mitochondrial dysfunction play a key role in the cascade of events leading to the degeneration of dopaminergic neurons typical of Parkinson's disease (Dias *et al*., 2013), and that in Alzheimer's disease activity of mitochondrial enzymes is significantly compromised as the antioxidant defense system (Luca *et al*., 2015). Furthermore, oxidative stress plays a central role in cancer onset, promoting epithelial-to-mesenchymal transition, cell migration, invasion, cell growth, survival and angiogenesis (Diebold & Chandel, 2016; Khan *et al*., 2021). Moreover, in literature it is reported that, in Nrf2 deficient mice, the downregulation of Nrf2 downstream genes makes mice more prone to develop skin cancer (Long *et al*., 2001), bladder (Iida *et al*., 2007), forestomach (Ramos-Gomez *et al*., 2001) and liver (Kitamura *et al*., 2006), indicating a protective role of Nrf2 against carcinogenesis. Consequently, using ROS scavenging or enhance antioxidant response, even through NRF2 pathway (Ali *et al*., 2023), are intriguing strategies proposed by many researchers to manage cancer (Cheung *et al*., 2020; C. Wang *et al*., 2018) and

neurodegenerative disorders (Gao *et al*., 2023; Newlanda *et al*., 2016). On the other hand, the aberrant activation of the NRF2 pathway has been linked to the onset of many types of tumors, especially non-small cell lung cancer (Scalera *et al*., 2022), since it can sustain tumor cell proliferation, migration (Gong *et al*., 2020) and drug resistance (Ghorbanhosseini *et al*., 2025; S. Wang *et al*., 2025). Furthermore, ROS can induce various forms of cell death, ranging from apoptosis to ferroptosis (Villalpando-Rodriguez & Gibson, 2021). Therefore, inhibition of antioxidant enzymes and the oxygen species-mediated DNA damage are even valid approaches for therapies (Fan *et al*., 2013; Sang *et al*., 2021). In this context, the modulation of MAPK15 may represent an interesting novel way to manage therapy and prevention of oxidative imbalance-correlated human diseases, since our current findings show that MAPK15 plays a key role in precisely regulating NRF2 activation in both normal and cancer cells, under basal conditions as well as in response to pro-oxidative stimuli.

Cigarette smoke is one of pro-oxidative stimuli to which we are massively exposed. According to the last estimates reported by World Health Organization (WHO) (https://iris.who.int/server/api/core/bitstreams/1903bfca-6c2f-470c-bd52-237edf4828ca/content), 1.2 million of people (≥ 15 years old) are smokers. It is widely recognized that cigarette smoke is a significant contributor to cancer, as well as to respiratory and cardiovascular conditions (Seo *et al*., 2023). Indeed, smoke contains a miscellaneous of chemical compounds including ROS, which can overload antioxidant cellular defense leading to oxidative stress that, as already mentioned, can be a trigger for tumorigenesis and other inflammatory related diseases (Caliri *et al*., 2021). From this consideration, we assessed the role of MAPK15 even in epithelial lung cells, both normal and cancerous, as they are the first cell type to be involved in smoke exposure. The present study demonstrates clearly that endogenous MAPK15 promotes antioxidant cellular defense also after CSE treatment in lung epithelial cells both normal and cancerous.

Although we demonstrated the ability of MAPK15 to support NRF2 antioxidant response upon CSE treatment in lung cells, mitigating DNA damage, we must consider that in epithelial cells of patients affected by chronic obstructive pulmonary disease, hyperactive MAPK15-ULK1 pathway exacerbates the disorder and, on the contrary, the inhibition of MAPK15-ULK1 signaling ameliorates the pathological phenotype (Zhang *et al*., 2021).

These awarenesses regarding bifunctional role both of NRF2 and MAPK15 in aggravating or mitigating diseases, suggest that, despite our reasonable confidence that MAPK15 dependent regulation of NRF2 is a general mechanism independent from cell types, the modulation of this kinase should be evaluated based on the pathological context. Another important aspect to be considered is how we can regulate the level of MAPK15. Indeed, pharmacological inhibitors of MAPK15 are already available or could be readily optimized (Strambi *et al*., 2013), although no compound capable of directly activating MAPK15 is currently known. This makes genetic strategies a more viable approach.

In conclusion, we presented a novel mechanism for cellular responses to oxidative stress based on NRF2 regulation by MAPK15. This kinase is able to enhance antioxidant cellular response following oxidative stress stimuli, promoting NRF2 transactivation via supporting protein stabilization and nuclear translocation. The upregulation of MAPK15, and the consequent maintenance of the antioxidant response, may be beneficial for the cell, as it protects against ROS and DNA damage (**Fig. 37**), thereby potentially preventing tumorigenesis, but it may be deleterious in some pathological context where NRF2 upregulation supports cancer development and drug resistance. For this reason, the biological context must always be considered.

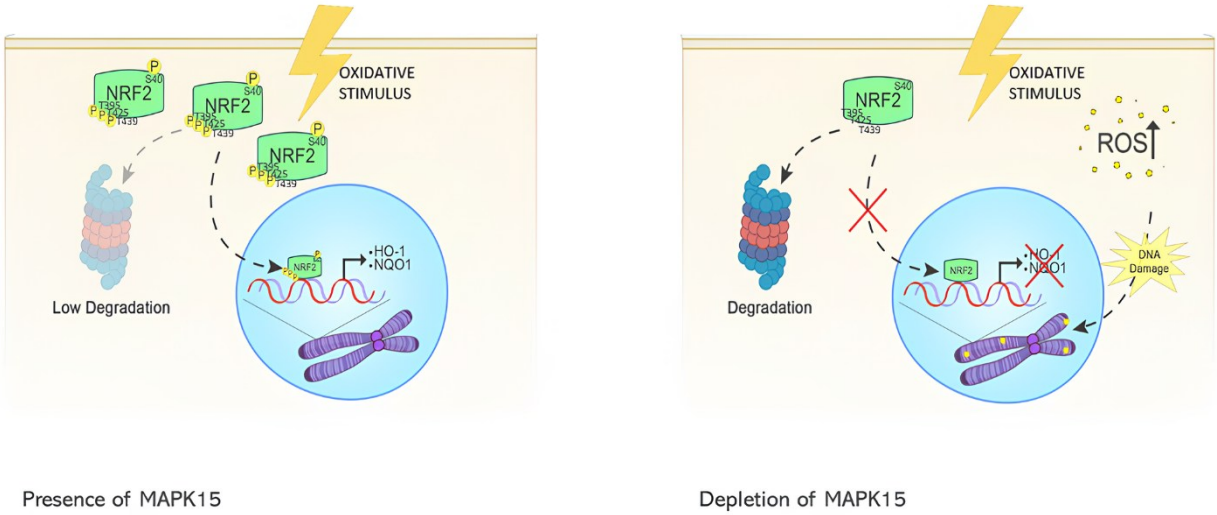

Fig. 37 Graphical model of MAPK15 regulation upon NRF2 and its biological consequence. When MAPK15 is present in cell, it supports NRF2 protein stabilization and nuclear translocation, promoting the translation of antioxidant genes, as HO-1 and NQO1, and protecting cell from DNA damage. When MAPK15 is depleted, NRF2 is degraded faster and its transactivation is not supported through MAPK15-dependent phosphorylations, leading to increment of ROS and genome instability.

6. Acknowledgement

I would like to thank Prof. Pietro Rubengi for being my tutor and for giving me the opportunity to start working in research, and Dr. Mario Chiariello for hosting me in his laboratory, including me in his working team and teaching me the basis of molecular biology and research.
In the end, I would like to thank my laboratory co-workers, Dr. Giovanni Inzalaco, Dr. Monia Taranta, Dr. Lisa Gherardini and Dr. Sara Gargiulo for helping me every single day and particularly Dr. Lorenzo Franci, without whom this research would not have been possible.

7. Bibliography

1. Abe, M. K., Kuo, W. L., Hershenson, M. B., & Rosner, M. R. (1999). Extracellular signal-regulated kinase 7 (ERK7), a novel ERK with a C-terminal domain that regulates its activity, its cellular localization, and cell growth. *Molecular and Cellular biology*, *19*(2), 1301-1312.

2. Abe, M. K., Kahle, K. T., Saelzler, M. P., Orth, K., Dixon, J. E., & Rosner, M. R. (2001). ERK7 is an autoactivated member of the MAPK family. *Journal of Biological Chemistry*, *276*(24), 21272-21279.

3. Abe, M. K., Saelzler, M. P., Espinosa, R., Kahle, K. T., Hershenson, M. B., Le Beau, M. M., & Rosner, M. R. (2002). ERK8, a new member of the mitogen-activated protein kinase family. *Journal of Biological Chemistry*, *277*(19), 16733-16743.

4. Alam, J., Stewart, D., Touchard, C., Boinapally, S., Choi, A. M., & Cook, J. L. (1999). Nrf2, a Cap'n'Collar transcription factor, regulates induction of the heme oxygenase-1 gene. *Journal of Biological Chemistry*, *274*(37), 26071-26078.

5. Ali, M. A., Khan, N., Kaleem, N., Ahmad, W., Alharethi, S. H., Alharbi, B., Alhassan, H. H., Al-Enazi, M. M., Razis, A. F. A., Modu, B., Calina, D., & Sharifi-Rad, J. (2023). Anticancer properties of sulforaphane: current insights at the molecular level. *Frontiers in oncology*, *13*, 1168321.

6. Baird, L., & Yamamoto, M. (2020). The Keap1-Nrf2 pathway: From mechanism to medical applications. In *Oxidative Stress* (pp. 125-147). Academic Press.

7. Bonora, M., Missiroli, S., Perrone, M., Fiorica, F., Pinton, P., & Giorgi, C. (2021). Mitochondrial control of genomic instability in cancer. *Cancers*, *13*(8), 1914.

8. Braicu, C., Buse, M., Busuioc, C., Drula, R., Gulei, D., Raduly, L., Rusu, A., Irimie, A., Atanasov, A. G., Slaby, O., Ionescu, C., & Berindan-Neagoe, I. (2019). A comprehensive review on MAPK: a promising therapeutic target in cancer. *Cancers*, *11*(10), 1618.

9. Caliri, A. W., Tommasi, S., & Besaratinia, A. (2021). Relationships among smoking, oxidative stress, inflammation, macromolecular damage, and cancer. *Mutation Research/Reviews in Mutation Research*, *787*, 108365.

10. Cargnello, M., & Roux, P. P. (2011). Activation and function of the MAPKs and their substrates, the MAPK-activated protein kinases. *Microbiology and molecular biology reviews*, *75*(1), 50-83.

11. Cheung, E. C., DeNicola, G. M., Nixon, C., Blyth, K., Labuschagne, C. F., Tuveson, D. A., & Vousden, K. H. (2020). Dynamic ROS control by TIGAR regulates the initiation and progression of pancreatic cancer. *Cancer cell*, *37*(2), 168-182.

12. Colecchia, D., Strambi, A., Sanzone, S., Iavarone, C., Rossi, M., Dall'Armi, C., Piccioni, F., Verrotti Di Pianella, A., & Chiariello, M. (2012). MAPK15/ERK8 stimulates autophagy by interacting with LC3 and GABARAP proteins. *Autophagy*, *8*(12), 1724-1740.

13. Davies, K. J. (1995, November). Oxidative stress: the paradox of aerobic life. In *Biochemical Society Symposia* (Vol. 61, pp. 1-31). Portland Press Limited.

14. Daiber, A., Kuntic, M., Hahad, O., Delogu, L. G., Rohrbach, S., Di Lisa, F., Schulz, R., & Münzel, T. (2020). Effects of air pollution particles (ultrafine and fine particulate matter) on mitochondrial function and oxidative stress–Implications for cardiovascular and neurodegenerative diseases. *Archives of biochemistry and biophysics*, *696*, 108662.

15. Dias, V., Junn, E., & Mouradian, M. M. (2013). The role of oxidative stress in Parkinson's disease. *Journal of Parkinson's disease*, *3*(4), 461-491.

16. Diebold, L., & Chandel, N. S. (2016). Mitochondrial ROS regulation of proliferating cells. *Free Radical Biology and Medicine*, *100*, 86-93.

17. Dymkowska, D. (2016). Oxidative damage of the vascular endothelium in type 2 diabetes-the role of mitochondria and NAD (P) H oxidase. *Postepy Biochem*, *62*(2), 116-126.

18. de Jager, T. L., Cockrell, A. E., & Du Plessis, S. S. (2017). Ultraviolet light induced generation of reactive oxygen species. *Ultraviolet light in human health, diseases and environment*, 15-23.

19. Dias, V., Junn, E., & Mouradian, M. M. (2013). The role of oxidative stress in Parkinson's disease. *Journal of Parkinson's disease*, *3*(4), 461-491.

20. Diebold, L., & Chandel, N. S. (2016). Mitochondrial ROS regulation of proliferating cells. *Free Radical Biology and Medicine*, *100*, 86-93.

21. Eggler, A. L., Small, E., Hannink, M., & Mesecar, A. D. (2009). Cul3-mediated Nrf2 ubiquitination and antioxidant response element (ARE) activation are dependent on the partial molar volume at position 151 of Keap1. *Biochemical journal*, *422*(1), 171-180.

22. Fan, C., Chen, J., Wang, Y., Wong, Y. S., Zhang, Y., Zheng, W., Cao, W., & Chen, T. (2013). Selenocystine potentiates cancer cell apoptosis induced by 5-fluorouracil by triggering reactive oxygen species-mediated DNA damage and inactivation of the ERK pathway. *Free Radical Biology and Medicine*, *65*, 305-316.

23. Filomeni, G., De Zio, D., & Cecconi, F. (2015). Oxidative stress and autophagy: the clash between damage and metabolic needs. *Cell Death & Differentiation*, *22*(3), 377-388.

24. Fogo, G. M., Raghunayakula, S., Emaus, K. J., Torres Torres, F. J., Wider, J. M., & Sanderson, T. H. (2024). Mitochondrial membrane potential and oxidative stress interact to regulate Oma1-dependent processing of Opa1 and mitochondrial dynamics. *The FASEB Journal*, *38*(18), e70066.

25. Franci, L., Tubita, A., Bertolino, F. M., Palma, A., Cannino, G., Settembre, C., Rasola, A., Rovida, E., & Chiariello, M. (2022). MAPK15 protects from oxidative stress-dependent cellular senescence by inducing the mitophagic process. *Aging Cell*, *21*(7), e13620.

26. Gao, W., Liu, W., Dong, X., & Sun, Y. (2023). Albumin–manganese dioxide nanocomposites: a potent inhibitor and ROS scavenger against Alzheimer's β-amyloid fibrillogenesis and neuroinflammation. *Journal of Materials Chemistry B*, *11*(43), 10482-10496.

27. Gerschman, R., Gilbert, D. L., Nye, S. W., Dwyer, P., & Fenn, W. O. (1954). Oxygen poisoning and x-irradiation: a mechanism in common. *Science*, *119*(3097), 623-626.

28. Ghorbanhosseini, S. S., Nourbakhsh, M., Mosaffa, F., & Aghaei, M. (2025). Targeting the PERK/NRF2 Pathway: Enhancing cisplatin Efficacy in Resistant Ovarian Cancer Cells through MRP1 and ROS Modulation. *Food and Chemical Toxicology*, 115672.

29. Gong, M., Li, Y., Ye, X., Zhang, L., Wang, Z., Xu, X., Shen, Y., & Zheng, C. (2020). Loss-of-function mutations in KEAP1 drive lung cancer progression via KEAP1/NRF2 pathway activation. *Cell Communication and Signaling*, *18*(1), 98.

30. Goodfellow, M. J., Borcar, A., Proctor, J. L., Greco, T., Rosenthal, R. E., & Fiskum, G. (2020). Transcriptional activation of antioxidant gene expression by Nrf2 protects against mitochondrial dysfunction and neuronal death associated with acute and chronic neurodegeneration. *Experimental neurology*, *328*, 113247.

31. Graves, J. D., Draves, K. E., Craxton, A., Saklatvala, J., Krebs, E. G., & Clark, E. A. (1996). Involvement of stress-activated protein kinase and p38 mitogen-activated protein kinase in mIgM-induced apoptosis of human B lymphocytes. *Proceedings of the National Academy of Sciences*, *93*(24), 13814-13818.

32. Groehler, A. L., & Lannigan, D. A. (2010). A chromatin-bound kinase, ERK8, protects genomic integrity by inhibiting HDM2-mediated degradation of the DNA clamp PCNA. *Journal of Cell Biology*, *190*(4), 575-586.

33. Han, Y. H., Kim, S. H., Kim, S. Z., & Park, W. H. (2009). Carbonyl cyanide p-(trifluoromethoxy) phenylhydrazone (FCCP) as an O2− generator induces apoptosis via the depletion of intracellular GSH contents in Calu-6 cells. *Lung Cancer*, *63*(2), 201-209.

34. Henrich, L. M., Smith, J. A., Kitt, D., Errington, T. M., Nguyen, B., Traish, A. M., & Lannigan, D. A. (2003). Extracellular signal-regulated kinase 7, a regulator of hormone-dependent estrogen receptor destruction. *Molecular and cellular biology*, *23*(17), 5979-5988.

35. Hurd, T. R., DeGennaro, M., & Lehmann, R. (2012). Redox regulation of cell migration and adhesion. *Trends in cell biology*, *22*(2), 107-115.

36. Iavarone, C., Acunzo, M., Carlomagno, F., Catania, A., Melillo, R. M., Carlomagno, S. M., Santoro, M., & Chiariello, M. (2006). Activation of the Erk8 mitogen-activated protein (MAP) kinase by RET/PTC3, a constitutively active form of the RET proto-oncogene. *Journal of Biological Chemistry*, *281*(15), 10567-10576.

37. Iida, K., Itoh, K., Maher, J. M., Kumagai, Y., Oyasu, R., Mori, Y., Shimazui, T., Akaza, H., & Yamamoto, M. (2007). Nrf2 and p53 cooperatively protect against BBN-induced urinary bladder carcinogenesis. *Carcinogenesis*, *28*(11), 2398-2403.

38. Jeon, S. J., Jung, G. H., Choi, E. Y., Han, E. J., Lee, J. H., Han, S. H., Woo, J. S., Jung, S. H., & Jung, J. Y. (2024). Kaempferol induces apoptosis through the MAPK pathway and regulates JNK-mediated autophagy in MC-3 cells. *Toxicological Research*, *40*(1), 45-55.

39. Jimenez-Blasco, D., Santofimia-Castaño, P., Gonzalez, A., Almeida, A., & Bolaños, J. P. (2015). Astrocyte NMDA receptors' activity sustains neuronal survival through a Cdk5–Nrf2 pathway. *Cell Death & Differentiation*, *22*(11), 1877-1889.

40. Khan, A. Q., Rashid, K., AlAmodi, A. A., Agha, M. V., Akhtar, S., Hakeem, I., Raza, S. S., & Uddin, S. (2021). Reactive oxygen species (ROS) in cancer pathogenesis and therapy: An update on the role of ROS in anticancer action of benzophenanthridine alkaloids. *Biomedicine & Pharmacotherapy*, *143*, 112142.

41. Kitamura, Y., Umemura, T., Kanki, K., Kodama, Y., Kitamoto, S., Saito, K., Itoh, K., Yamamoto., M., Masegi, T., Nishikawa, A., & Hirose, M. (2007). Increased susceptibility to hepatocarcinogenicity of Nrf2-deficient mice exposed to 2-amino-3-methylimidazo [4, 5-f] quinoline. *Cancer science*, *98*(1), 19-24.

42. Klevernic, I. V., Stafford, M. J., Morrice, N., Peggie, M., Morton, S., & Cohen, P. (2006). Characterization of the reversible phosphorylation and activation of ERK8. *Biochemical Journal*, *394*(1), 365-373.

43. Kobayashi, M., & Yamamoto, M. (2006). Nrf2–Keap1 regulation of cellular defense mechanisms against electrophiles and reactive oxygen species. *Advances in enzyme regulation*, *46*(1), 113-140.

44. Kovac, S., Angelova, P. R., Holmström, K. M., Zhang, Y., Dinkova-Kostova, A. T., & Abramov, A. Y. (2015). Nrf2 regulates ROS production by mitochondria and NADPH oxidase. *Biochimica et Biophysica Acta (BBA)-General Subjects*, *1850*(4), 794-801.

45. Kwak, M. K., Itoh, K., Yamamoto, M., & Kensler, T. W. (2002). Enhanced expression of the transcription factor Nrf2 by cancer chemopreventive agents: role of antioxidant response element-like sequences in the nrf2 promoter. *Molecular and cellular biology*, *22*(9), 2883-2892.

46. Li, Y. A., Chen, H. Y., Hsieh, C. P., Chen, C. L., Hung, S. C., & Huang, Y. F. (2023). Acute generation of reactive oxygen species that induced by doxycycline pretreatment results in rapid cell death in polyphyllin G-treated osteosarcoma cell lines. *Environmental Toxicology*, *38*(5), 1174-1184.

47. Li, B., Ming, H., Qin, S., Nice, E. C., Dong, J., Du, Z., & Huang, C. (2025). Redox regulation: mechanisms, biology and therapeutic targets in diseases. *Signal Transduction and Targeted Therapy*, *10*(1), 72.

48. Liu, W., Lin, M., Dai, Y., & Hong, F. (2024). Hypoxia Activates FGF-23-ERK/MAPK Signaling Pathway in Ischemia-Reperfusion-Induced Acute Kidney Injury. *Kidney and Blood Pressure Research*, *49*(1), 933-945.

49. Long, D. J., Waikel, R. L., Wang, X. J., Roop, D. R., & Jaiswal, A. K. (2001). NAD (P) H: quinone oxidoreductase 1 deficiency and increased susceptibility to 7, 12-dimethylbenz [a]-anthracene-induced carcinogenesis in mouse skin. *Journal of the National Cancer Institute*, *93*(15), 1166-1170.

50. Luca, M., Luca, A., & Calandra, C. (2015). The role of oxidative damage in the pathogenesis and progression of Alzheimer's disease and vascular dementia. *Oxidative medicine and cellular longevity*, *2015*(1), 504678.

51. Newland, B., Wolff, P., Zhou, D., Wang, W., Zhang, H., Rosser, A., Wang, W., & Werner, C. (2016). Synthesis of ROS scavenging microspheres from a dopamine containing poly (β-amino ester) for applications for neurodegenerative disorders. *Biomaterials science*, *4*(3), 400-404.

52. Nit, K., Tyszka-Czochara, M., & Bobis-Wozowicz, S. (2021). Oxygen as a master regulator of human pluripotent stem cell function and metabolism. *Journal of Personalized Medicine*, *11*(9), 905.

53. Ozturk, T., Mignot, J., Gattazzo, F., Gervais, M., Relaix, F., Rouard, H., & Didier, N. (2024). Dual inhibition of P38 MAPK and JNK pathways preserves stemness markers and alleviates premature activation of muscle stem cells during isolation. *Stem Cell Research & Therapy*, *15*(1), 179.

54. Pagano, M. A., Bain, J., Kazimierczuk, Z., Sarno, S., Ruzzene, M., Di Maira, G., Elliott, M., Orzeszko, A., Cozza, G., Meggio, F., & Pinna, L. A. (2008). The selectivity of inhibitors of protein kinase CK2: an update. *Biochemical Journal*, *415*(3), 353-365.

55. Parascandolo, A., Benincasa, G., Corcione, F., & Laukkanen, M. O. (2024). ERK2 Is a Promoter of Cancer Cell Growth and Migration in Colon Adenocarcinoma. *Antioxidants*, *13*(1), 119.

56. Piasecki, B. P., Sasani, T. A., Lessenger, A. T., Huth, N., & Farrell, S. (2017). MAPK-15 is a ciliary protein required for PKD-2 localization and male mating behavior in Caenorhabditis elegans. *Cytoskeleton*, *74*(10), 390-402.

57. Ramos-Gomez, M., Kwak, M. K., Dolan, P. M., Itoh, K., Yamamoto, M., Talalay, P., & Kensler, T. W. (2001). Sensitivity to carcinogenesis is increased and chemoprotective efficacy of enzyme inducers is lost in nrf2 transcription factor-deficient mice. *Proceedings of the National Academy of Sciences*, *98*(6), 3410-3415.

58. Rosette, C., & Karin, M. (1996). Ultraviolet light and osmotic stress: activation of the JNK cascade through multiple growth factor and cytokine receptors. *Science*, *274*(5290), 1194-1197.

59. Rossi, M., Colecchia, D., Iavarone, C., Strambi, A., Piccioni, F., Di Pianella, A. V., & Chiariello, M. (2011). Extracellular signal-regulated kinase 8 (ERK8) controls estrogen-related receptor α

(ERRα) cellular localization and inhibits its transcriptional activity. *Journal of Biological Chemistry*, *286*(10), 8507-8522.

60. Rossi, M., Colecchia, D., Ilardi, G., Acunzo, M., Nigita, G., Sasdelli, F., Celetti, A., Strambi, A., Staibano, S., Croce, C. M., & Chiariello, M. (2016). MAPK15 upregulation promotes cell proliferation and prevents DNA damage in male germ cell tumors. *Oncotarget*, *7*(15), 20981.

61. Saelzler, M. P., Spackman, C. C., Liu, Y., Martinez, L. C., Harris, J. P., & Abe, M. K. (2006). ERK8 down-regulates transactivation of the glucocorticoid receptor through Hic-5. *Journal of Biological Chemistry*, *281*(24), 16821-16832.

62. Sang, J., Li, W., Diao, H. J., Fan, R. Z., Huang, J. L., Gan, L., Zou, M. F., Tang, G. H., & Yin, S. (2021). Jolkinolide B targets thioredoxin and glutathione systems to induce ROS-mediated paraptosis and apoptosis in bladder cancer cells. *Cancer Letters*, *509*, 13-25.

63. Sarniak, A., Lipińska, J., Tytman, K., & Lipińska, S. (2016). Endogenous mechanisms of reactive oxygen species (ROS) generation. *Postepy higieny i medycyny doswiadczalnej (Online)*, *70*, 1150-1165.

64. Scalera, S., Mazzotta, M., Cortile, C., Krasniqi, E., De Maria, R., Cappuzzo, F., Ciliberto, G., & Maugeri-Saccà, M. (2022). KEAP1-mutant NSCLC: the catastrophic failure of a cell-protecting hub. *Journal of Thoracic Oncology*, *17*(6), 751-757.

65. Seo, Y. S., Park, J. M., Kim, J. H., & Lee, M. Y. (2023). Cigarette smoke-induced reactive oxygen species formation: a concise review. *Antioxidants*, *12*(9), 1732.

66. Shi, Y., Huang, M., Zhou, W., Zhao, Y., Zhao, J., Zhong, B., French, S. W., Tang, X., & Liu, H. (2025). TGF-β/JNK axis mediates mitochondrial damage and macrophage cGAS-STING activation in liver Mallory-Denk body pathogenesis. *Journal of Translational Medicine*, *23*(1), 621.

67. Shin, J. N., Rao, L., Sha, Y., Abdel Fattah, E., Hyser, J., & Eissa, N. T. (2021). p38 MAPK activity is required to prevent hyperactivation of NLRP3 inflammasome. *The Journal of Immunology*, *207*(2), 661-670.

68. Strambi, A., Mori, M., Rossi, M., Colecchia, D., Manetti, F., Carlomagno, F., Botta, M., & Chiariello, M. (2013). Structure prediction and validation of the ERK8 kinase domain. *PloS one*, *8*(1), e52011.

69. Tonelli, C., Chio, I. I. C., & Tuveson, D. A. (2018). Transcriptional regulation by Nrf2. *Antioxidants & redox signaling*, *29*(17), 1727-1745.

70. Van Der Reest, J., Lilla, S., Zheng, L., Zanivan, S., & Gottlieb, E. (2018). Proteome-wide analysis of cysteine oxidation reveals metabolic sensitivity to redox stress. *Nature communications*, *9*(1), 1581.

71. Vara, D., & Pula, G. (2014). Reactive oxygen species: physiological roles in the regulation of vascular cells. *Current molecular medicine*, *14*(9), 1103-1125.

72. Vessoni, A. T., Filippi-Chiela, E. C., Menck, C. F., & Lenz, G. (2013). Autophagy and genomic integrity. *Cell Death & Differentiation*, *20*(11), 1444-1454.

73. Villalpando-Rodriguez, G. E., & Gibson, S. B. (2021). Reactive oxygen species (ROS) regulates different types of cell death by acting as a rheostat. *Oxidative Medicine and Cellular Longevity*, *2021*(1), 9912436.

74. Wakabayashi, N., Itoh, K., Wakabayashi, J., Motohashi, H., Noda, S., Takahashi, S., Imakado, S., Kotsuji, T., Otsuka, F., Roop D. R., Harada, T., Engel, J. D., & Yamamoto, M. (2003). Keap1-null mutation leads to postnatal lethality due to constitutive Nrf2 activation. *Nature genetics*, *35*(3), 238-245.

75. Wang, C., Wang, J., Zhang, X., Yu, S., Wen, D., Hu, Q., Ye, Y., Bomba, H., Hu, X., Liu, Z., Dotti, G., & Gu, Z. (2018). In situ formed reactive oxygen species–responsive scaffold with gemcitabine and checkpoint inhibitor for combination therapy. *Science translational medicine*, *10*(429), eaan3682.

76. Wang, W., Yang, H., Fan, Z., & Shi, R. (2024). NQO1 promotes osteogenesis and suppresses angiogenesis in DPSCs via MAPK pathway modulation. *Stem Cell Research & Therapy*, *15*(1), 306.

77. Wang, S., Zhang, C., Zhou, S., Liu, S., Li, Q., Cheng, X., Wang, R., Chen, B., Li, Y., & Xi, M. (2025). RNF217-KEAP1-NRF2 feedback loop confers therapeutic resistance by inhibiting ferroptosis in esophageal squamous cell carcinoma. *Drug Resistance Updates*, 101296.

78. Wu, X., Wei, J., Yi, Y., Gong, Q., & Gao, J. (2022). Activation of Nrf2 signaling: A key molecular mechanism of protection against cardiovascular diseases by natural products. *Frontiers in pharmacology*, *13*, 1057918.

79. Xu, Y. M., Zhu, F., Cho, Y. Y., Carper, A., Peng, C., Zheng, D., Yao, K., Lau, A. T. Y., Zykova, T. A., Kim, H. G., Bode, A. M., & Dong, Z. (2010). Extracellular signal-regulated kinase 8–mediated c-Jun phosphorylation increases tumorigenesis of human colon cancer. *Cancer research*, *70*(8), 3218-3227.

80. Yagishita, Y., Fukutomi, T., Sugawara, A., Kawamura, H., Takahashi, T., Pi, J., Uruno, A., & Yamamoto, M. (2014). Nrf2 protects pancreatic β-cells from oxidative and nitrosative stress in diabetic model mice. *Diabetes*, *63*(2), 605-618.

81. Yeang, H. X. A., Hamdam, J. M., Al-Huseini, L. M., Sethu, S., Djouhri, L., Walsh, J., Kitteringham, N., Park, B. K., Goldring, C. E., & Sathish, J. G. (2012). Loss of transcription factor nuclear factor-erythroid 2 (NF-E2) p45-related factor-2 (Nrf2) leads to dysregulation of immune functions, redox homeostasis, and intracellular signaling in dendritic cells. *Journal of Biological Chemistry*, *287*(13), 10556-10564.

82. Zhang, M., Fang, L., Zhou, L., Molino, A., Valentino, M. R., Yang, S., Zhang, J., Li, Y., & Roth, M. (2021). MAPK15-ULK1 signaling regulates mitophagy of airway epithelial cell in chronic obstructive pulmonary disease. *Free Radical Biology and Medicine*, *172*, 541-549.

8. Web bibliography

1. https://www.kinase-screen.mrc.ac.uk

2. https://iris.who.int